Geochemistry Geophysics Geosystems G3

Article
Volume 12, Number 6
22 June 2011
Q06009, doi:10.1029/2011GC003592
ISSN: 1525-2027

Published by AGU and the Geochemical Society

Structure and serpentinization of the subducting Cocos plate offshore Nicaragua and Costa Rica

H. J. A. Van Avendonk
Jackson School of Geosciences, University of Texas Institute for Geophysics, Austin, Texas 78722, USA (harm@utig.ig.utexas.edu)

W. S. Holbrook
Department of Geology and Geophysics, University of Wyoming, Laramie, Wyoming 82071, USA

D. Lizarralde
Department of Geology and Geophysics, Woods Hole Oceanographic Institution, Woods Hole, Massachusetts 02543, USA

P. Denyer
Escuela Centroamericana de Geología, University of Costa Rica, San Pedro 214-2060, Costa Rica

[1] The Cocos plate experiences extensional faulting as it bends into the Middle American Trench (MAT) west of Nicaragua, which may lead to hydration of the subducting mantle. To estimate the along strike variations of volatile input from the Cocos plate into the subduction zone, we gathered marine seismic refraction data with the R/V *Marcus Langseth* along a 396 km long trench parallel transect offshore of Nicaragua and Costa Rica. Our inversion of crustal and mantle seismic phases shows two notable features in the deep structure of the Cocos plate: (1) Normal oceanic crust of 6 km thickness from the East Pacific Rise (EPR) lies offshore Nicaragua, but offshore central Costa Rica we find oceanic crust from the northern flank of the Cocos Nazca (CN) spreading center with more complex seismic velocity structure and a thickness of 10 km. We attribute the unusual seismic structure offshore Costa Rica to the midplate volcanism in the vicinity of the Galápagos hot spot. (2) A decrease in Cocos plate mantle seismic velocities from ~7.9 km/s offshore Nicoya Peninsula to ~6.9 km/s offshore central Nicaragua correlates well with the northward increase in the degree of crustal faulting outboard of the MAT. The negative seismic velocity anomaly reaches a depth of ~12 km beneath the Moho offshore Nicaragua, which suggests that larger amounts of water are stored deep in the subducting mantle lithosphere than previously thought. If most of the mantle low velocity zone can be interpreted as serpentinization, the amount of water stored in the Cocos plate offshore central Nicaragua may be about 2.5 times larger than offshore Nicoya Peninsula. Hydration of oceanic lithosphere at deep sea trenches may be the most important mechanism for the transfer of aqueous fluids to volcanic arcs and the deeper mantle.

Components: 14,900 words, 15 figures.

Keywords: Central America; Cocos Plate; Galápagos hot spot; plate bending and faulting; seismic velocities; subduction.

Index Terms: 3025 Marine Geology and Geophysics: Marine seismics (0935, 7294); 8138 Tectonophysics: Lithospheric flexure; 8170 Tectonophysics: Subduction zone processes (1031, 3060, 3613, 8413).

Received 28 February 2011; **Revised** 21 April 2011; **Accepted** 21 April 2011; **Published** 22 June 2011.

Van Avendonk, H. J. A., W. S. Holbrook, D. Lizarralde, and P. Denyer (2011), Structure and serpentinization of the subducting Cocos plate offshore Nicaragua and Costa Rica, *Geochem. Geophys. Geosyst.*, *12*, Q06009, doi:10.1029/2011GC003592.

1. Introduction

[2] The subduction of oceanic lithosphere causes flexural bending of downgoing plates near deep sea trenches. Analyses of bathymetry and gravity profiles show that bending stresses can exceed the strength of the oceanic lithosphere, causing a reduction of the flexural rigidity near convergent plate boundaries [*Caldwell et al.*, 1976]. Compression in the lower half of the subducting plate may manifest itself as ductile shortening [*McNutt and Menard*, 1982], whereas extension of the more brittle oceanic crust leads to normal faulting [*Chapple and Forsyth*, 1979; *Ranero et al.*, 2005] that can be mapped on the seafloor outboard the trenches [*Masson*, 1991]. In seismic reflection images across the Middle American Trench (MAT), *Ranero et al.* [2003] showed that these faults extend from the seafloor into the oceanic upper mantle.

[3] The new faults that break the oceanic crust at the outer rise and trench of subduction zones provide pathways for seawater into the crust and underlying mantle. In this setting, hydrothermal circulation [*Langseth and Silver*, 1996] facilitates chemical reactions that form water rich rocks such as serpentinite [*Ranero and Sallarès*, 2004]. Since serpentinite is much weaker than the peridotite it replaces [*Escartín et al.*, 2001], hydration of the lithosphere will lower its mechanical strength near the trench axis [*Faccenda et al.*, 2009]. Deeper in the subduction zone, the presence of water influences slip behavior near the plate interface [*Davis et al.*, 1983; *Moore and Saffer*, 2001], and it is critically important for arc magmatism [*Stolper and Newman*, 1994; *Schmidt and Poli*, 1998]. The depth at which volatiles are discharged from a subducting slab will depend on the pressures and temperatures they encounter during the descent [*Peacock et al.*, 2005]. Since the oceanic mantle of the subducting plate is relatively insulated from the overlying, hot mantle wedge, it is likely that much of the water that is stored deep in the downgoing slab will be released at arc magmatic depths or deeper in the mantle [*Hacker*, 2008; *van Keken et al.*, 2011].

[4] In recent years, marine seismologists have gathered more evidence for deep fracturing and hydration of the oceanic lithosphere near the trench axis. Imaging of the deep structure offshore Central America [*Grevemeyer et al.*, 2007; *Ivandic et al.*, 2008, 2010] and South America [*Ranero and Sallarès*, 2004; *Contreras-Reyes et al.*, 2008a] with ocean bottom seismometer (OBS) refraction profiles has shown that seismic wave speeds are reduced in both the oceanic crust and upper mantle between the outer rise of the subduction zone and the trench axis. Although the depth of serpentinization in the downgoing lithosphere may not be well constrained yet by these studies, we now have compelling evidence from these geophysical studies that it is caused by bending and fracturing of the subducting plate.

[5] The MAT offshore Nicaragua and Costa Rica is one location where we can investigate the processes of brittle deformation and hydrothermal alteration of the oceanic lithosphere during subduction (Figure 1). In the north, the Cocos plate dips steeply beneath Nicaragua [*Protti et al.*, 1994], the seafloor outboard of the trench is pervasively faulted [*Ranero et al.*, 2003], and the strike of these faults corresponds well with the orientation of nodal planes of local earthquake focal mechanisms [*Ranero et al.*, 2005]. Fault scarps are not as prominent on the seafloor southward along the trench axis, suggesting that a fault controlled mechanism of crustal and upper mantle alteration should be less effective offshore central Costa Rica.

[6] The apparent difference in faulting and hypothesized fault related hydration of the incoming plate between central Nicaragua and central Costa Rica should have an effect on magmatic processes in the overlying mantle wedge. A seismic low velocity zone on top of the subducting slab beneath Nicaragua is interpreted as direct evidence of water release into the mantle wedge beneath the arc [*Abers et al.*, 2003]. Tomographic images of Vp/Vs [*Syracuse et al.*, 2008] and seismic attenuation [*Rychert et al.*, 2008] suggest that the devolatization of the wet slab beneath the mantle wedge of Nicaragua leads to more hydrous melting here than beneath Costa Rica. Geochemical indicators, such as Ba/La and B/La ratios from arc lavas [*Noll et al.*, 1996; *Patino et al.*, 2000; *Carr et al.*, 2003], are consistent with a larger input of slab derived fluids beneath Nicaragua than beneath Costa Rica, but the true origin of these geochemical trends is still debated [*Carr et al.*, 2007].

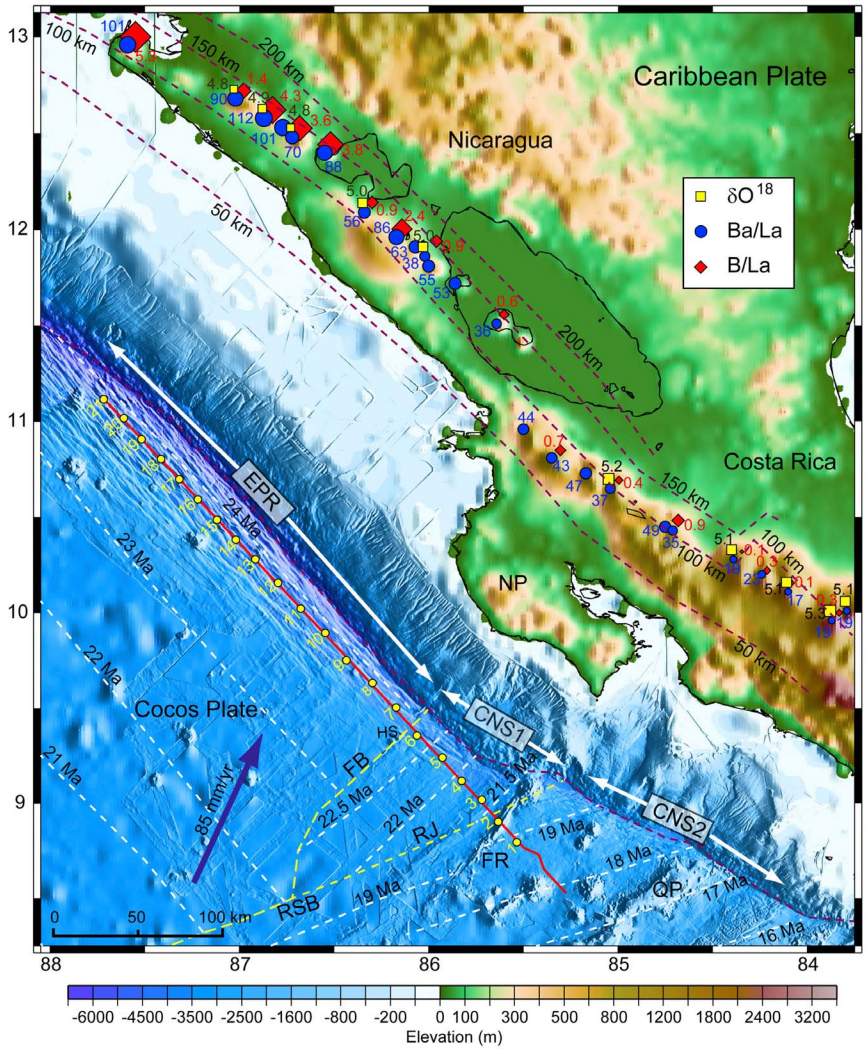

Figure 1. Elevation map of our study area, the Pacific margin of Nicaragua and Costa Rica. Shown on land are depth contours (labeled dashed lines) of the surface of the subducting slab [*Syracuse and Abers*, 2006] and three geochemical indicators of slab signature in arc lavas, averaged for individual volcanic centers: Blue circles show the Ba/La ratios [*Carr et al.*, 2003], yellow squares show δO^{18} in ‰ [*Eiler et al.*, 2005], and red diamonds indicate B/La [*Leeman et al.*, 1994]; symbol size is proportional to values. Offshore, yellow dashed lines mark the rough-smooth boundary (RSB), Farallon Breakup (FB) trace, and the ridge jump (RJ) between the CNS1 and CNS2 segments of the Cocos-Nazca spreading center. White dashed lines indicate seafloor ages according to *Barckhausen et al.* [2001]. NP, Nicoya Peninsula; HS, Hernando Scarp; FR, Fisher Ridge; QP, Quepos Plateau. The red line shows the ship track with air gun shots for line SERP. Yellow circles are the positions of OBSs used for this seismic refraction study.

[7] In this study we present an analysis of marine seismic refraction data acquired on the Cocos plate offshore Costa Rica and Nicaragua. The resultant seismic velocity model shows that the oceanic lithosphere is likely more faulted and hydrothermally altered offshore Nicaragua than offshore Costa Rica. In addition we image thicker than normal oceanic crust offshore central Costa Rica, which indicates that the Galápagos hot spot has caused excess volcanism over a wide area on the Cocos plate. The effects of midplate volcanism and bending related faulting of the Cocos plate may explain some of the first order differences in subduction zone geometry and arc lava geochemistry between Costa Rica and Nicaragua.

2. Geological Setting

2.1. Seafloor Spreading History

[8] The history of seafloor spreading offshore Costa Rica and Nicaragua is fairly well constrained

by magnetic anomalies on the adjacent Cocos plate [*Barckhausen et al.*, 2001] and on conjugate sections of oceanic crust elsewhere in the Pacific [*Lonsdale*, 2005; *Barckhausen et al.*, 2008]. Oceanic crust of the Farallon plate formed at the EPR west of Central America until about 23 Ma ago, when an east west fissure started to break this plate into the modern Cocos plate to the north, and the Nazca plate to the south. This tear in the lithosphere, marked by the Farallon breakup (FB) discontinuity (Figure 1), propagated eastward from the EPR to the Galapagos hot spot track, probably exploiting it as a zone of weakness [*Barckhausen et al.*, 2008]. The fissure eventually reached the MAT, by ~19.5 Ma according to *Barckhausen et al.* [2008], fully separating the Cocos and Nazca plates. The Cocos Nazca (CN) spreading center that initiated in the wake of the rupture has changed its orientation a few times in its subsequent history [*Meschede et al.*, 1998], but overall it has accreted Cocos plate crust in a northward direction [*Hey*, 1977]. The seafloor spreading history explains the variations in the age and character of the subducting Cocos plate along the strike of the MAT between central Nicaragua and central Costa Rica. Offshore northern Costa Rica and Nicaragua lies ~24 Ma old oceanic crust that was produced at the EPR, which is slightly older than the age of breakup of the Farallon plate [*Barckhausen et al.*, 2001]. The EPR crust is bending into the MAT in the paleospreading direction, such that bend faulting reactivates the abyssal hill fabric [*Ranero et al.*, 2005]. The Hernando Scarp, which lies at the southeastern boundary of the EPR segment near the trench (Figure 1), is thought to be an old flank of the Farallon plate fissure [*Lonsdale*, 2005]. Southeast of this boundary lies an 80 km wide segment (CNS1 in Figure 1) with southwest northeast trending magnetic anomalies, which is consistent with accretion of oceanic crust at a spreading center parallel to the eastward propagating fissure. *Lonsdale* [2005] and *Barckhausen et al.* [2001] give somewhat different ages for the CNS1 crust offshore Nicoya Peninsula, but they agree that by 19.5 Ma the Cocos Nazca spreading center reoriented to a more north south spreading direction (CNS2 in Figure 1).

[9] The seafloor of the CNS2 segment decreases in age from ~19.5 Ma south of Nicoya Peninsula to less than 15 Ma offshore Osa Peninsula. Seamounts and larger volcanic plateaus, which are common here, date to ~14 Ma [*Werner et al.*, 2003], considerably younger than the underlying oceanic crust. The presence of these volcanic highs is generally attributed to the passage of the Cocos plate over the Galápagos hot spot, which produced the ~19 km thick Cocos Ridge in its trace [*Sallarès et al.*, 2003; *Walther*, 2003]. Over the last 20 Ma, the center of the Galápagos hot spot was never far from the CN spreading center [*Sallarès and Charvis*, 2003], so excess magmatism may have produced thicker than normal oceanic crust at the CN spreading center in addition to off axis underplating of young CN crust.

2.2. Arc Geochemical Trends

[10] Lavas from the Central American arc exhibit systematic variations in fluid mobile isotope and trace element abundances over distances of a few hundred kilometers along the convergent margin. For example, Ba/La ratios are as large as 101 ± 8 in northwestern Nicaragua, but they decrease to 9 ± 2 in central Costa Rica [*Carr et al.*, 2003] (Figure 1). Similar large scale trends can be observed in B/La [*Leeman et al.*, 1994; *Noll et al.*, 1996], ^{10}Be10/^{9}Be [*Tera et al.*, 1986; *Morris et al.*, 1990] and δ^{18}O [*Eiler et al.*, 2005]. The rich inventory of trace elements and isotopes in marine sediments of the incoming plate has a large influence on arc lava geochemistry [*Plank and Langmuir*, 1998]. The sediment cover on the Cocos plate offshore Central America is almost uniformly 400 m [*Shipboard Scientific Party*, 1979, 1998], but ^{10}Be/^{9}Be ratios from the volcanic front show that a larger portion of the near surface sediments is subducted offshore Nicaragua than offshore Costa Rica [*Cardace and Morris*, 2009]. Perhaps the fault scarps that form by bending of the Cocos plate offshore central and northwestern Nicaragua help to entrain more sediment [*Kelly*, 2003]. The carbonates and hemipelagic sediments of the downgoing plate are also rich in Ba and B, which helps explain the increase of Ba/La and B/La in arc lavas from Costa Rica to Nicaragua [*Patino et al.*, 2000] (Figure 1). However, between central and western Nicaragua volcanic rocks the B/La ratio increases considerably more than Ba/La, which *Patino et al.* [2000] attribute to the mobilization and recycling of boron from altered oceanic crust of the Cocos plate.

[11] If most of the pore water in the underthrusting sediments and upper crust is expelled from the downgoing plate beneath the forearc of Costa Rica [*Ranero et al.*, 2008; *Sahling et al.*, 2008; *Van Avendonk et al.*, 2010], hydrous fluids stored in the slab mantle may be the primary agent by which fluid mobile elements are transferred from marine sediments to the overlying mantle wedge [*You et al.*, 1996; *Tenthorey and Hermann*, 2004]. The breakdown of serpentinites from the subducting slab

under increasing temperature and pressure likely delivers large amounts of water to the plate boundary at arc magmatic depths [*Schmidt and Poli*, 1998; *Hacker et al.*, 2003b]. There may therefore be a causal relationship between the degree of serpentinization in the oceanic mantle of the Cocos plate near the trench and the abundance of ^{10}Be, Ba and B in arc lavas of Costa Rica and Nicaragua [*Rüpke et al.*, 2002]. Measured values of δ^{18}O along the volcanic front of southern Central America may be inversely correlated with slab hydration, since water released from subducted serpentinites is diluted in ^{18}O [*Eiler et al.*, 2005].

[12] The along arc geochemical trends are consistent with a relatively wet slab beneath Nicaragua [*Abers et al.*, 2003], but there are other factors to consider: 1) The steeper slab beneath Nicaragua would be expected to discharge its volatiles in a relatively narrow column beneath the volcanic front, leading to more concentrated hydrous fluxing of the mantle wedge here than beneath central Costa Rica, even if the total amount of released H_2O does not vary along the plate boundary [*Carr et al.*, 2007; *Bolge et al.*, 2009]. 2) Regional variations in element ratios such as Ba/La and B/La may be influenced by La heterogeneity in the subarc mantle [*Morris and Hart*, 1983]. A strong decrease in La abundance from central Costa Rica northward toward Nicaragua may be the result of enrichment of the mantle wedge beneath Costa Rica under the influence of the Galápagos hot spot [*Carr et al.*, 1990, 2007]. 3) Arc extrusives account for only about 13% of the total magmatic and volatile flux [*Sadofsky et al.*, 2008] in southern Central America, so the abundance of fluid mobile elements in arc volcanic rocks would not have to correlate strongly with H_2O input from the downgoing slab. Recent studies of olivine fluid inclusions from the Central American arc [*Wade et al.*, 2006; *Sadofsky et al.*, 2008] confirm that Ba/La and B/La ratios correlate well with H_2O content of parental magmas, but for the above reasons *Sadofsky et al.* [2008] do not claim evidence for a large regional difference in the total H_2O budget between the Costa Rican and Nicaragua arc segments. To test the relationship between these geochemical indicators and the H_2O supply to the Central American subduction zone we need better constraints on along strike variations in the hydration of the subducting Cocos plate.

[13] Some isotopic and trace element concentrations in the volcanic arc of Central America correlate well with the composition of oceanic crust, seamounts and plateaus of the subducting Cocos plate [*Feigenson et al.*, 2004; *Hoernle et al.*, 2008]. For example, La/Yb ratios are >10 in both the modern Galápagos province and in central Costa Rica, but they are less than 4 in Nicaragua [*Gazel et al.*, 2009]. Subduction of Cocos Ridge, the prominent trace of the Galápagos hotpot on the Cocos plate, has left an ocean island basalt (OIB) imprint on the arc geochemistry of central Costa Rica [*Hoernle et al.*, 2008] over at least the last 8 Ma [*Gazel et al.*, 2009]. The seamounts and plateaus northwest of Cocos Ridge, such as Quepos Plateau and Fisher Ridge, also have distinct OIB geochemical characteristics [*Werner et al.*, 2003; *Sadofsky et al.*, 2009] that may be reproduced in arc lavas of northwestern Costa Rica [*Gazel et al.*, 2009] and in the backarc region as far as the southern Nicaragua Rise [*Janoušek et al.*, 2010; *Gazel et al.*, 2011]. The dispersion of the OIB signature northwest from central Costa Rica toward the Nicaragua segment of the volcanic arc may be facilitated by asthenospheric flow along the plate boundary [*Herrstrom et al.*, 1995; *Hoernle et al.*, 2008]. To understand the arc parallel transport of this OIB component we must have a good definition of the lateral extent of Galápagos hot spot volcanism on the Cocos plate.

3. Seismic Data

[14] In the Spring of 2008 we conducted a multichannel seismic (MCS) reflection and OBS refraction experiment with the R/V *Marcus Langseth* to characterize the structure of the Cocos plate near the MAT. Previous seismic refraction studies of the Cocos plate have shown compelling evidence for serpentinization offshore Nicaragua [e.g., *Ivandic et al.*, 2010] and thickened oceanic crust offshore central Costa Rica [e.g., *Sallarès et al.*, 2003], but the resultant seismic refraction lines were too short to investigate structural variations in the subducting plate along the strike of the margin over several hundred km. We therefore acquired a 396 km long transect, referred to as SERP, parallel to the MAT between Costa Rica and Nicaragua (Figure 2). The northern 260 km of this seismic line lies near the 24 Ma isochron on crust of the EPR segment, at a distance of 15–20 km from the trench axis. The southern portion of the line lies on crust with ages between 22.7 and 18 Ma that was produced at the CNS1 and CNS2. The paleospreading direction here is approximately parallel or oblique to the seismic transect (Figure 1). Key objectives for the analysis of transect SERP are 1) the fracturing and alteration of the Cocos plate lithosphere near the

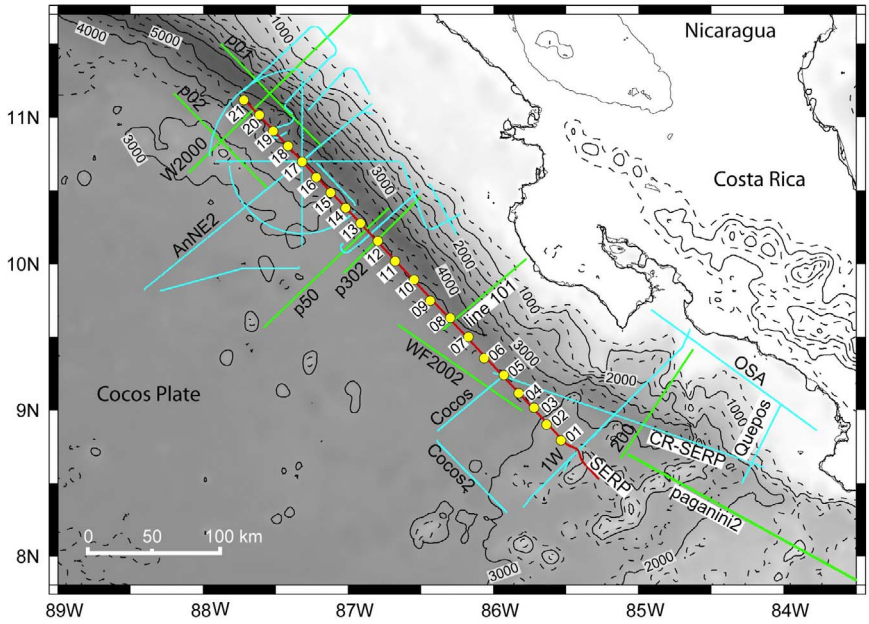

Figure 2. Gray scale bathymetry map with older (green) and new TICOCAVA (light blue) seismic refraction profile locations, which also includes line SERP (red). Yellow circles are labeled OBS locations in this study. Published OBS seismic refraction profiles are W2000 [*Walther et al.*, 2000], p50 [*Ivandic et al.*, 2008], p302 [*Grevemeyer et al.*, 2007], p01 and p02 [*Ivandic et al.*, 2010], 101 [*Christeson et al.*, 1999; *Sallarès et al.*, 2001], 200 [*Ye et al.*, 1996], WF2002 [*Walther and Flueh*, 2002], and Paganini2 [*Sallarès et al.*, 2003; *Walther*, 2003].

MAT, and 2) differences in crustal structure between the EPR, CNS1 and CNS2 segments.

[15] We used two ships to acquire the seismic reflection and refraction data for transect SERP. The R/V *New Horizon* deployed 21 instruments from the U.S. OBS Instrument Pool (OBSIP) with an average spacing of 18 km. No OBSs were deployed on the southern 45 km of SERP, so we do not have reversed data coverage there. The R/V *Marcus Langseth* deployed its 108 L air gun array to shoot the refraction line with a 500 m spacing, which corresponds to an average shot interval of 200 s. This large interval was sufficient to reduce the previous shot noise at very large source receiver distances [*Christeson et al.*, 1996]. The R/V *Marcus Langseth* also towed an 8 km long streamer, even though the shot spacing was not appropriate for detailed seismic reflection imaging.

[16] During the acquisition of seismic transect SERP, which was carried out from southeast to northwest, we encountered two minor problems: Soon after the start of the shoot, the R/V *Marcus Langseth* made a deviation of ~2 km from the planned SERP transect to avoid a fishing vessel south of instrument OBS 1 (Figure 2). Later in the experiment, on a 17 km wide stretch in the vicinity of instrument OBS 5, we ramped down the air gun array of the R/V *Marcus Langseth* due the presence of sea turtles. After the seismic shoot, all OBSs were recovered, and they recorded data on four components for the duration of the experiment. Unfortunately, only the hydrophone data were of sufficient quality to interpret in this study. The signal to noise ratio on the three orthogonal seismometers was consistently lower than on the hydrophone channel. Perhaps as a result we have very few observations of shear waves, but we recorded useful compressional waves from our air gun shots on all instruments.

[17] The 21 OBS receiver gathers on line SERP gave us a total of 5777 travel time picks, consisting of 2244 crustal turning compressional waves (Pg), 300 reflections from within the oceanic crust (PiP) of the CNS1 and CNS2 segments, 913 Moho reflections (PmP), and 2320 mantle refraction (Pn) arrival times. The gather of instrument OBS 14 (Figure 3) shows how we identified crustal and mantle arrivals in the hydrophone data. All travel times and their uncertainties were picked visually in the OBS record sections. We used seafloor multiples to verify the arrival times of long offset refractions, and we checked reciprocity with other source-receiver pairs in our data set. We recorded Pg arrivals to distances of 25 km to 45 km on most

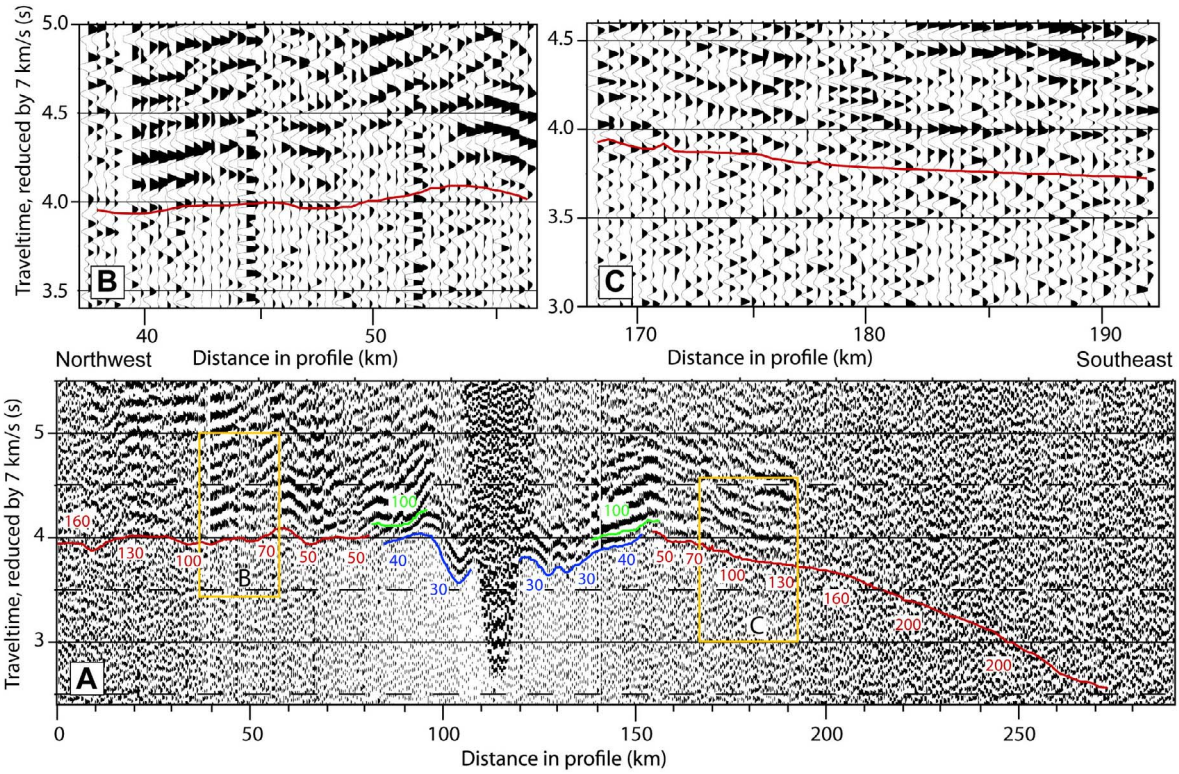

Figure 3. Example of seismic refraction data from line SERP. (a) Hydrophone record from OBS 14, which is located at 114 km from the northwest on line SERP. The vertical axis is reduced by 7 km/s. At near offsets the direct wave from air gun shots to the OBS can be seen at 2.7 s. At larger offsets we identify the crustal turning wave Pg travel times (blue), Moho reflections PmP (green) and mantle refractions Pn (red). The labels show the assigned travel time uncertainties, which increase with source-receiver offset. Orange boxes indicate insets. (b) Detail of seismic refraction data shot northwest of OBS 14. (c) Detail of data shot the southeast.

OBSs, and Pn arrivals at larger offsets. Near the Pg/Pn crossover distance we also observed PmP arrivals and PiP arrivals on CN crust. The travel time uncertainties increase significantly with source-receiver distance, from 30 ms within 20 km of the instruments to 200 ms over offsets larger than 100 km (Figure 3). The distribution of travel time picks over different source-receiver offsets peaks at 25–30 km (Figure 4) because we observe most PmP arrivals at these distances, in addition to Pg and Pn arrivals. At larger offsets we have fewer travel time picks, and these long-offset arrival times have larger uncertainties due to their lower signal-to-noise ratio.

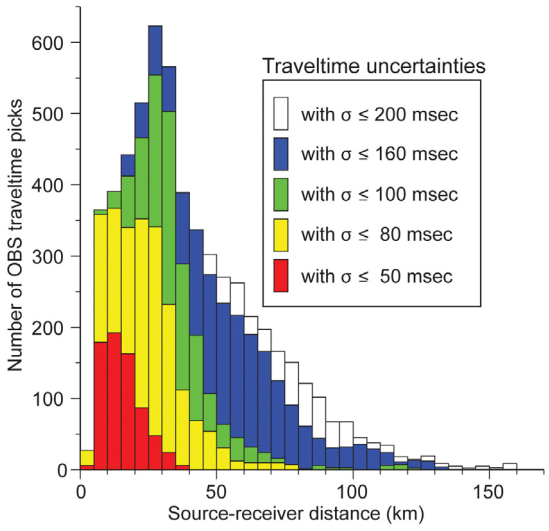

Figure 4. Histograms show the distribution of source-receiver offsets for all OBS refraction travel times. The range distribution is shown for travel time picks within error bounds (see color legend). The histograms show that travel time picks at large offsets generally have larger uncertainties.

4. Results

4.1. Tomography

[18] The seismic structure of the Cocos plate crust and upper mantle along line SERP is constrained with wide-angle seismic travel times from our 21 OBSs. In this section we describe the inversion

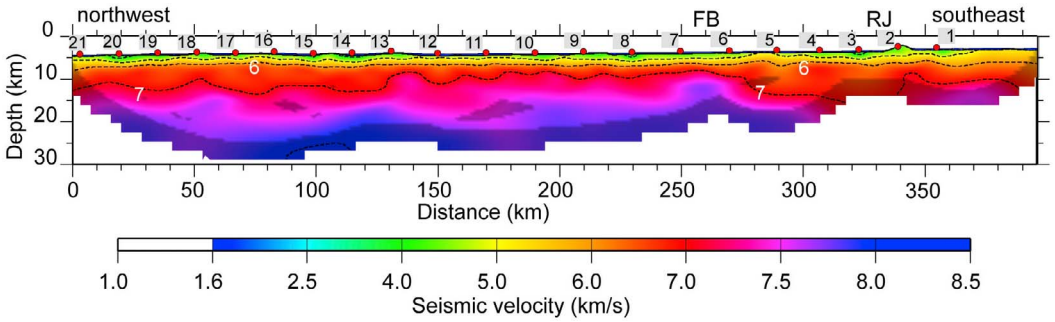

Figure 5. Result of a travel time inversion of first-arriving phases (Pg and Pn) for seismic velocity structure of the oceanic crust and upper mantle along line SERP. Black dashed lines are 1.0 km/s seismic velocity contours. Dark shades on the velocity model cover parts of the model that are not sampled by raypaths.

of the travel time data for a 2-D seismic velocity profile along our seismic transect. We calculate the resolution and covariance matrices to determine the quality of different parts of our model. Last, we discuss variations in seismic structure of the Cocos plate along seismic transect SERP.

[19] As a first step in our analysis of the data from line SERP we determine the depth of the top of the basement. The seafloor of the Cocos plate offshore Costa Rica and Nicaragua is covered by carbonates and hemipelagic sediment, punctuated by a few seamounts and ridges. We can constrain the thickness of the sediment layer with the streamer shot gathers recorded by the R/V *Marcus Langseth* during the seismic refraction experiment. Because of the large shot spacing (500 m) we do not stack the streamer data. Instead we estimate the depth of basement beneath air gun shots by forward modeling of basement reflections in shot gathers. Our analysis confirms earlier marine seismic studies [*Shipley and Moore*, 1986] and drilling [*Coulbourn et al.*, 1982; *Shipboard Scientific Party*, 1998] which have shown that the thickness of this sediment cover is uniformly 350 m to 400 m along the MAT, with seismic velocities of 1.7 to 2.0 km/s.

[20] To find a seismic velocity model that fits our OBS data we alternate between ray tracing and linear inversions of the travel time residuals. We trace raypaths and calculate travel times between the air gun shot and OBS locations with the shortest path method [*Moser*, 1991] and ray bending [*Moser et al.*, 1992; *Van Avendonk et al.*, 2001]. Subsequently we scale travel time residuals with pick uncertainties, and invert them for a new seismic velocity model. Each linearized inversion gives us an update in seismic velocities and the depth of model boundaries. We repeat ray tracing and linear inversions until the model perturbations have become small, and the travel time misfit is within an acceptable range [*Van Avendonk et al.*, 1998, 2004].

[21] Since the interpretation of crustal and mantle phases in our travel time data set (see previous section) is a fairly subjective step [*Zelt et al.*, 2003], we first carry out an inversion of 4564 first-arriving phases (Pg and Pn). With the travel times of first-arriving turning waves we can create a smooth image of the seismic velocity structure beneath the basement surface. In Figure 5 we show the result of this preliminary inversion, where we achieve a root-mean-square misfit of 80 ms for the first-arriving travel time picks. The resultant seismic velocity model shows a clear lateral change in the lithospheric structure at the FB discontinuity, which crosses our profile at 260 km. To the northwest, where the seafloor is produced at the EPR (Figure 1), the seismic velocities increase rapidly with depth from 4 km/s near the basement to 6 km/s at 2 km beneath the basement. At larger depth we see a steady decrease of seismic velocities to the northwest. Southeast of the FB discontinuity, where the crust formed at the incipient CN spreading center, seismic velocities are generally lower. Possibly the crust is thicker here, although the Moho is not defined in this model. To constrain the Moho boundary we need to use PmP travel times.

[22] To incorporate the observed PiP and PmP phases in our inversion, we define a model with Moho discontinuity across our entire model and a midcrustal boundary southeast of the FB discontinuity (Figure 1). The PiP arrivals in our OBS data suggest a two-layer crust along the CN segment to the southeast, whereas no such midcrustal phases were observed on EPR crust to the northwest. Our inversion of wide-angle reflection and refraction travel times simultaneously constrains the seismic velocities and boundary depths along the profile of transect SERP. After fifteen iterations of ray tracing

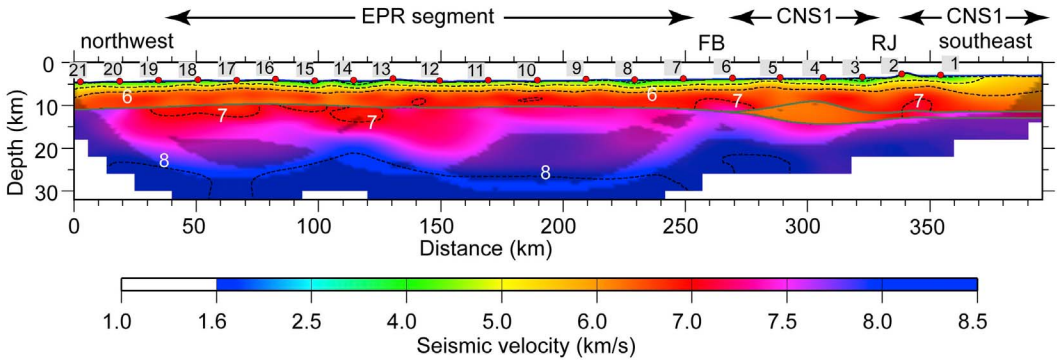

Figure 6. Final seismic velocity model, the result of an inversion of wide-angle seismic reflections and refractions of all OBSs along line SERP. Seismic velocities and shading as in Figure 5. Gray lines are the midcrustal reflector at the southeast end of the line and the Moho, which were both adjusted in the inversion.

and linear inversion we obtain a layered seismic velocity model (Figure 6) that fits our 5,777 OBS travel time picks with a root-mean-square misfit of 61 ms, and a normalized χ^2 misfit of 0.7. The very good data fit indicates that our assignment of travel time picking uncertainties may have been too conservative.

[23] Our final tomographic model achieves a very good average data fit, particularly for the crustal refractions (Pg). These crustal turning waves provide good ray coverage for the crustal layer in our seismic velocity model (Figure 7). Some of the long-offset PmP and Pn phases show a data misfit of 150–200 ms (Figure 7), which is consistent with the larger travel time pick uncertainty that we assigned to these arrivals (Figure 4). We show the travel time fits and ray diagrams for a number of individual OBS records in Section 1 of the Text S1 of the auxiliary material.[1]

4.2. Resolution

[24] Although the quality of our seismic refraction data from transect SERP was fairly consistent, the coverage of our seismic velocity model is not even. The crustal layer is largely covered with raypaths from Pg and deeper phases (Figure 7). The Pn arrivals sample the mantle of the EPR segment (between 0 km and 260 km in Figure 7) to depths of 25 km below sea level, but coverage of the mantle of the CNS1 and CNS2 segments is much sparser and it does not extend far beneath the Moho. We can quantify the ray coverage with the derivative weight sum (DWS), which represents the influence of all data on each model parameter in our final inversion [*Toomey and Foulger*, 1989]. In our profile of transect SERP, the DWS is generally higher in the crust than in the mantle (Figure 8) owing to the smaller uncertainties in crustal refractions. The Moho is sampled more evenly on the EPR segment than on the CN portion of our seismic transect. The midcrustal boundary in the CN crust is better defined than the Moho beneath the thick CN crust at 300 km in our model.

[25] The DWS gives a good first indication of the ray coverage in different parts of our preferred model, but the ability of our inversion to constrain seismic structure is better expressed with the resolution matrix, which we derive from the generalized inverse [*Van Avendonk et al.*, 2004]. In parts of our model that are well covered by raypaths we expect that the resolution matrix approaches the identity matrix [*Menke*, 1984], which means that the velocity image is not much distorted. In areas where ray coverage is poor, the resolution matrix should show that our imaged seismic velocity structure is averaged over large distances.

[26] Given the increase in travel time uncertainties with source/receiver distance on all our OBS records (Figure 4), we expect much better resolution in the oceanic crust of the Cocos plate than in the underlying mantle. In our first resolution test we investigate how well our data can resolve model features of 8 km wide by 3 km high. In a second test, we increase the size of this averaging window to 16 km wide by 6 km high. In each of these two tests, we slide an elliptical window of fixed dimensions over our model to see how well this object is imaged (Figure 9) [*Van Avendonk et al.*, 2004]. Values between 0.0 and 1.0 indicate that this structure is either poorly or well resolved. We would consider a value of 0.5 a fairly good result, although the

[1]Auxiliary materials are available in the HTML. doi:10.1029/2011GC003592.

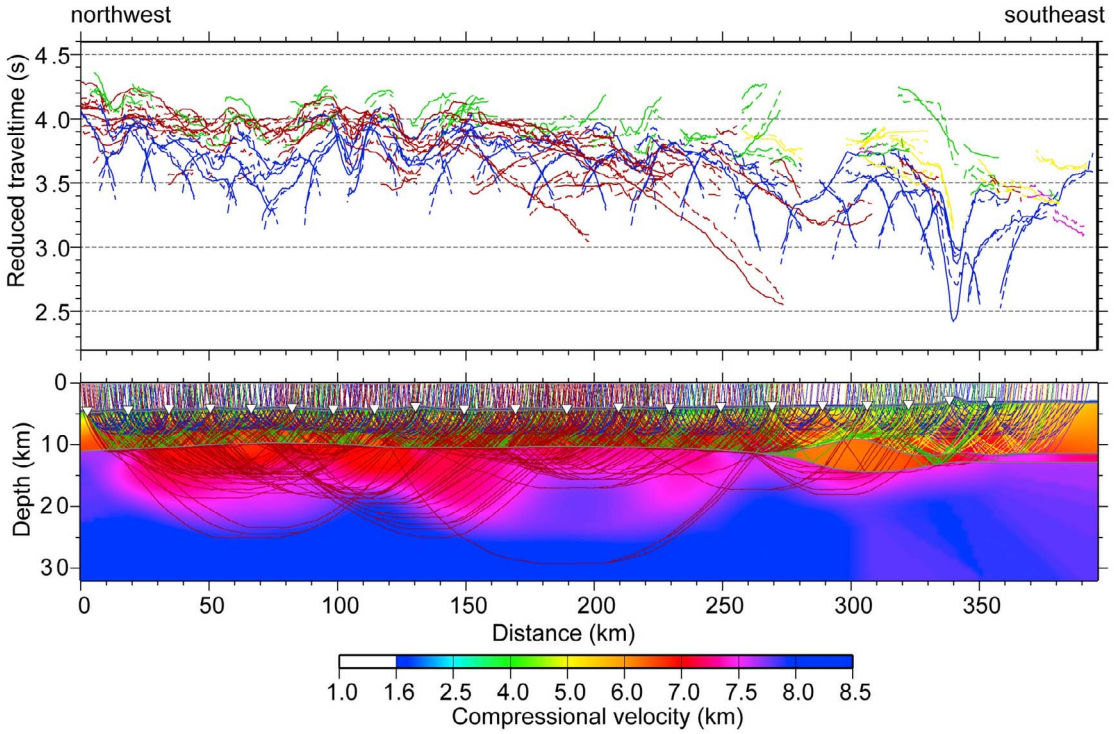

Figure 7. Ray diagram and travel time fits for all OBSs on line SERP. For the observed travel time phases we use the same color as in Figure 5. Solid travel time curves represent picks, and dashed travel time curves are calculated by our ray-tracing program.

magnitude of seismic velocity anomalies may be underestimated.

[27] Our first test shows that seismic velocity anomalies of 8 km by 3 km in the oceanic crust along transect SERP are adequately resolved, with the exception of the lower crust around 300 km, and toward the southwestern end of our model (Figure 9, top). The lower oceanic crust between 290 km and 320 km represents a low-velocity anomaly with poor ray coverage. The uppermost

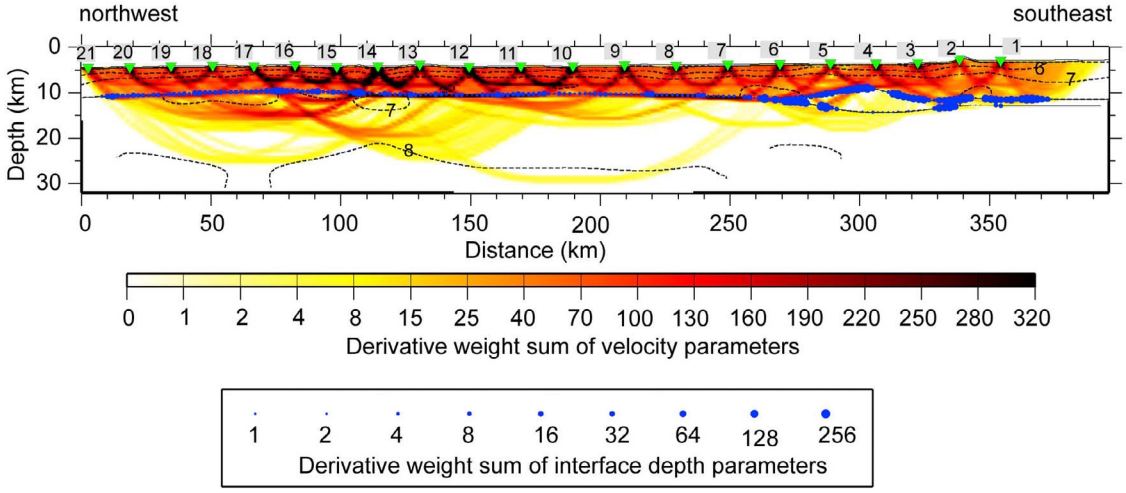

Figure 8. Derivative weight sum (DWS) for the last iteration of the travel time inversion. The largest ray densities are achieved in the crustal layer, and in the vicinity of the OBSs. The DWS is lowest deeper in the mantle due to low ray densities and larger travel time uncertainties for the large offset raypaths that sample the lower portion of the model. DWS coverage of the reflecting boundaries in the inversion is shown with blue dotted lines. As the scale indicates, the thicker blue lines represent denser coverage of the reflecting boundaries.

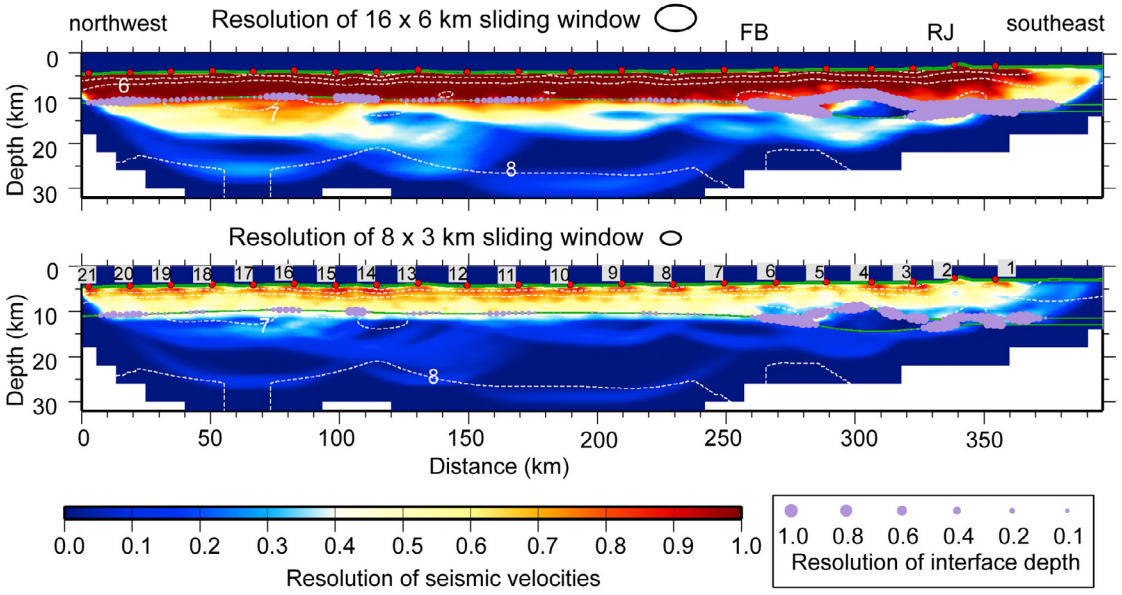

Figure 9. Resolving power of the inversion estimated from the full resolution matrix. We multiply the resolution matrix with a (top) 16 km by 6 km elliptical sliding window and (bottom) 8 km by 3 km sliding window to estimate how much of this object can be resolved by tomographic inversion. Resolution values of 0.5 are considered sufficient to image features of the size of the sliding window. The purple dotted lines show the resolution of reflecting boundaries in the model.

mantle shows adequate resolution at this small length scale due to the coverage with Pn head waves, but deeper in the mantle the resolution values are small. Variations in crustal thickness over distances of 8 km are mostly poorly resolved, although some crustal boundaries at the southeast end of our velocity model can be recovered (Figure 9, top).

[28] Lateral variations in the seismic velocity of the Cocos plate upper mantle may be resolved better on a scale of 16 km (horizontal) by 6 km (vertical). With this larger averaging window, it appears that in the upper 10 km of the mantle, mostly between depths of 10 km to 20 km, we obtain resolution values near 0.5. We therefore assume that our model (Figure 6) is a good representation of the seismic structure of the Cocos plate along transect SERP, though seismic velocities in the mantle represent averages over approximately10 km to 20 km. We computed the a posteriori covariance matrix [*Menke*, 1984] for our final inversion (Section 2 of Text S1 of the auxiliary material), which indicates that the uncertainty in Moho depth may be as large as 1.3 km, but seismic velocities are generally resolved with a standard deviation less than 0.1 km/s.

4.3. Seismic Velocity Structure

[29] The seismic velocity model of the crust and upper mantle along line SERP shows a number of features that are not typical of fast spreading oceanic lithosphere. The crustal thickness of the EPR segment is approximately 6 km, which is comparable to other studies here [*Ivandic et al.*, 2010], but the crust of the CNS1 segment, which is bounded by the FB and RJ magnetic age discontinuities (Figure 6), has a poorly constrained thickness of 9 km to 11 km. Farther southeast, the crust of the CNS2 segment may be 8–9 km thick. Unfortunately, our wide-angle data coverage of line SERP southeast of 360 km is unreversed, so this portion of the model is not well constrained.

[30] As *Grevemeyer et al.* [2007] and *Ivandic et al.* [2008] have reported previously, the seismic velocities in the Cocos plate offshore Nicaragua are lower than average for ~24 Ma EPR lithosphere [*White et al.*, 1992]. A comparison of 1-D seismic profiles from our SERP model with three 1-D profiles from seismic refraction lines across the MAT [*Christeson et al.*, 1999; *Walther et al.*, 2000; *Ivandic et al.*, 2008] shows that we image the lowest seismic velocities in the EPR segment of the Cocos plate parallel to the MAT (Figure 10). This apparent azimuthal variation in mantle seismic velocity could be caused by intrinsic anisotropy inherited during the formation of oceanic lithosphere [*Hess*, 1964]. Alternatively, we must consider that the orientation of transect SERP along the MAT was more favorable for constraining the magnitude of

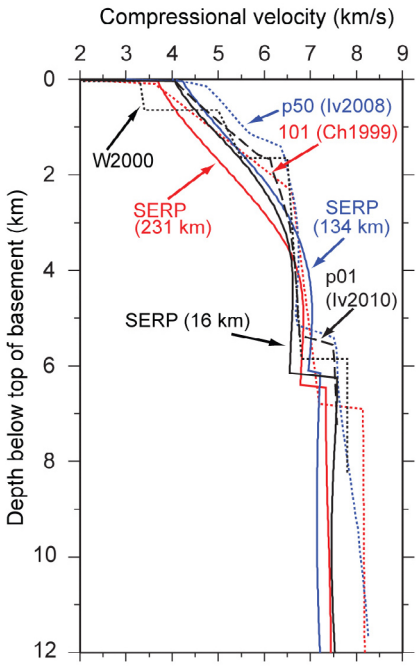

Figure 10. Comparison of 1-D vertical velocity profiles from the EPR along transect SERP with other seismic velocity models from the Cocos plate at the MAT. For the location of all seismic transects see Figure 2. Solid lines represent profiles extracted from our SERP model, while dotted lines are 1-D profiles extracted from seismic lines across the MAT. The refraction transect of *Walther et al.* [2000] offshore northwestern Nicaragua (black), line p50 [*Ivandic et al.*, 2008] offshore southwestern Nicaragua (red), and line 101 [*Christeson et al.*, 1999] offshore Nicoya Peninsula (red) resulted in seismic velocities that are lower than our SERP model. The trench-parallel seismic line p01 [*Ivandic et al.*, 2010] offshore northwestern Nicaragua (black dashed line) resulted in seismic velocities that are fairly similar to our SERP model.

the seismic low-velocity anomaly, which may be relatively narrow perpendicular to the trench. The studies of *Christeson et al.* [1999] and *Walther et al.* [2000] covered only a small portion of the Cocos plate across the MAT, so they probably did not record sufficient long-offset arrivals on the downgoing plate to image its deep structure. Even the seismic refraction line p50 (Figure 2) shows seismic velocities between 7.6 and 7.8 km/s (Figure 10) in the shallow mantle beneath the MAT offshore southwestern Nicaragua [*Ivandic et al.*, 2008], where we obtained mantle seismic velocities as low as 7.2 km/s. The trench-parallel OBS refraction line of *Ivandic et al.* [2010] found seismic velocities of ~7.3 km/s offshore northwestern Nicaragua, which is more similar to our result (Figure 10).

[31] Our inversion of reflection and refraction arrivals (Figure 6) confirms our observation from the first-arrival inversion (Figure 5) that the seismic velocities of CN crust is significantly lower than the velocities of the EPR crust. Between 260 km and 320 km, our tomographic inversion produced a low seismic velocity anomaly in the lower crust of the CNS1 segment using reflection and refraction travel times (Figure 6). However, the first-arrival inversion (Figure 5) does not show as much variation of seismic velocity with depth in the upper 10 km. Imaging a negative velocity gradient with surface-to-surface seismic data is generally very difficult, because raypaths largely diffract around regions of low seismic velocity (Figure 7). Our resolution analysis (Figure 9) also indicates that we should be careful interpreting this low-velocity anomaly in our reflection and refraction tomography model. The true nature of the crust of the CNS1 segment may be more complex than the seismic velocity structure imaged between the FB and RJ discontinuities in our two models (Figures 5 and 6).

[32] According to our SERP model, the 8–9 km thick crust of the CNS1 segment of the Cocos plate has a low vertical velocity gradient (Figure 6). A 1-D velocity profile at 360 km in our model of transect SERP (Figure 11) shows a fairly linear increase from 4.0 km/s near the basement surface to roughly 5.8 km/s at 3 km depth. In the lower crust the seismic velocity gradually increases to ~6.8 km/s. Previous seismic refraction studies in this area [*Ye et al.*, 1996; *Sallarès et al.*, 2003; *Walther*, 2003] are largely consistent with our results. Compared to our good constraints on the mantle seismic structure of the EPR segment, we only sample mantle seismic velocities in the first ~2 km beneath CN crust (Figure 11). The mantle seismic velocities of ~7.8 km/s here are comparable to those imaged by *Walther* [2003].

5. Discussion

5.1. Crustal Accretion of the Cocos Plate

[33] Our seismic velocity model of transect SERP shows a contrast between the crust produced at the EPR and CN oceanic spreading centers (Figures 6 and 11). The EPR crust is normal in thickness and structure, which suggests that the process of seafloor spreading at this mid-ocean ridge prior to the breakup of the Farallon plate was not significantly different from the mode of crustal accretion at the modern, fast spreading EPR. In contrast, the

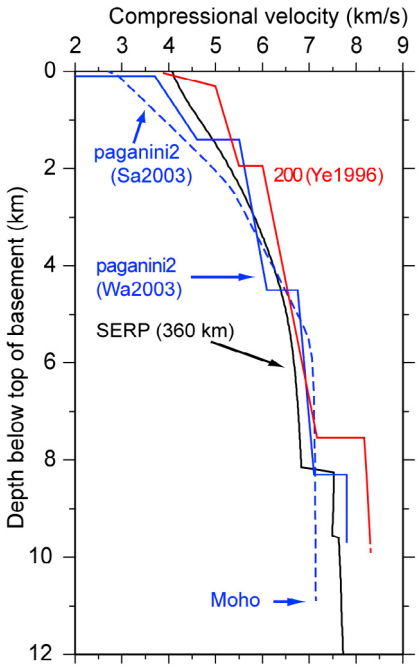

Figure 11. Vertical velocity profiles from southeast end of transect SERP near instrument OBS 1 (black line) and nearby published seismic velocity models from the CNS2 segment. For the location of seismic transects see Figure 2. The 1-D profile at the seaward end of line 200 [*Ye et al.*, 1996] (red line) lies just 30 km east of line SERP. In approximately the same location we have 1-D profiles from the northwest end of the Paganini2 OBS transect, which has been interpreted independently by *Sallarès et al.* [2003] (blue dashed line) and *Walther* [2003] (blue solid line).

crust of the CNS1 segment has a thickness of 10–11 km, and the seismic velocity of its lower crust (6.3 km/s) is very unusual for oceanic crust. An OBS seismic line just 20–25 km farther from the trench [*Walther and Flueh*, 2002] (WF2002 in Figure 2) also showed thicker oceanic crust and a low-velocity lens beneath 22–22.5 Ma old seafloor of the CNS1 segment (Figure 1). A comparison with line SERP shows that their low-velocity anomaly is much smaller than in our model, but it is similarly located at the base of the oceanic crust (Figure 12). *Walther and Flueh* [2002] suggest that the anomaly is a relict magma chamber, rather than a section of serpentinized mantle, because the outline of the lens is well constrained by wide-angle seismic refractions. Our OBS refraction data cannot rule out the possibility that this low-velocity anomaly on transect SERP is either an igneous body or a portion of serpentinized mantle.

[34] If the low-velocity lens in the CNS1 segment is part of the lower oceanic crust, it would have a composition that is much more felsic than what we find at a normal mid-ocean ridge. Since the anomaly lies just southeast of the ~23.5 Ma FB discontinuity [*Barckhausen et al.*, 2008], *Walther and Flueh* [2002] proposed that a short-lived magma chamber may have formed it at the southeastern edge of the ruptured EPR lithosphere. Although felsic rocks have only been found in small quantities in mid-ocean ridge systems, anatexis of gabbroic crust under hydrous conditions could produce silicic melts [*Koepke et al.*, 2007]. Perhaps the infiltration of seawater during the rupture of Farallon lithosphere facilitated melting and differentiation of the lower crust before the new CN spreading center was established. Alternatively, the low-velocity anomaly may be a section of mantle that was serpentinized during breakup of the Farallon plate.

[35] The seismic structure of the CNS2 segment is not well resolved in our profile of line SERP, mainly because the OBS refraction data at the southwest end of the profile are not reversed (Figure 7). The 8 km thick oceanic crust of the CNS2 segment near Fisher Ridge appears quite similar to the seismic structure of the Quepos plateau on the Paganini2 profile (Figure 11) [*Sallarès et al.*, 2003; *Walther*, 2003]. Since the oceanic crust here formed in the vicinity of the Galápagos hot spot, plume melts may have migrated to the young CN ridge axis to form thicker crust, such as can be observed at the modern Galápagos spreading center [*Canales et al.*, 2002]. The crust of the CNS2 segment may also

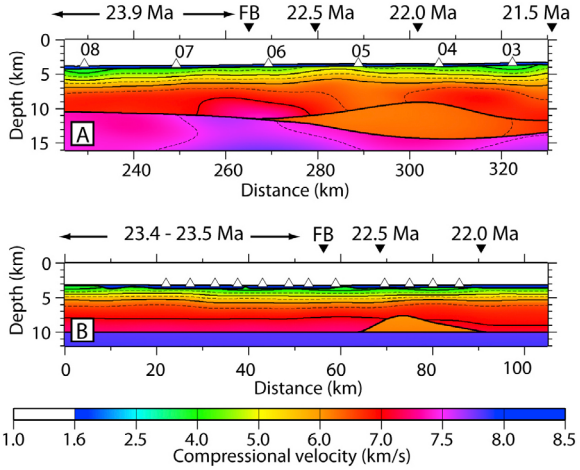

Figure 12. (a) Detail of our velocity model of line SERP across Farallon breakup trace (FB), with low-velocity anomaly in lower crust to the southeast. White triangles are OBS locations. Seafloor ages according to *Barckhausen et al.* [2001]. (b) Seismic velocity model of *Walther and Flueh* [2002] on a subparallel seismic transect (Figure 2).

have thickened significantly off axis. The seafloor offshore central Costa Rica is characterized by seamounts and fairly large plateaus, whose age is mostly 14 Ma [*Werner et al.*, 1999], while the underlying seafloor is thought to be a few million years older [*Barckhausen et al.*, 2001]. Seismic reflection images show layering of the igneous basement near the seamounts [*von Huene et al.*, 2000], which may represent flood basalts that presumably were emplaced off axis.

[36] The seismic velocity of the uppermost mantle beneath the CNS1 and CNS2 segments appears to be 7.7–7.8 km/s (Figures 6 and 11), which is lower than for normal oceanic mantle. *Walther* [2003] found the same low mantle velocity on line Paganini2 (Figure 2) across Quepos Plateau, so this feature may be widespread on the CNS2 segment. Two possible explanations for such low mantle seismic velocities may be a small amount of mantle serpentinization or melt retention beneath the oceanic Moho. Both processes have been documented mostly in studies of ocean crust produced at cool, slow-spreading ridges [*Lizarralde et al.*, 2004]. The CNS2 spreading center formed new crust at a half rate of 35 mm/yr [*Barckhausen et al.*, 2001], which could be considered an intermediate to fast spreading rate. Melt may have been retained in the shallow mantle near the Galápagos hot spot if melt production outpaced melt extraction during the early history of the CNS2 segment. *Walther* [2003] found similarly low mantle seismic velocities beneath the north flank of Cocos Ridge, which he also interpreted to be the result of melt retention during interaction between Galápagos plume and the young CN spreading center. The oceanic mantle northwest of the Cocos Ridge may also be enriched [*Hoernle et al.*, 2000], which could lead to lower mantle seismic velocities, though such an effect is assumed to be small [*Schutt and Lesher*, 2006]. Alternatively, it is possible that bending of the Cocos plate causes serpentinization, even as far as 30 km or 40 km outside the MAT, although the bathymetry (Figure 1) does not suggest that the lithosphere at the south end of transect SERP is faulting under bending stresses (Section 5.2).

5.2. Bending and Fracturing of the Cocos Plate

[37] We discuss how the degree of faulting and embrittlement of the incoming plate may vary along transect SERP. Bending of an oceanic plate near a trench can lead to a reduction in the seismic velocities through two different processes [e.g., *Contreras-Reyes et al.*, 2008b; *Ivandic et al.*, 2008]: 1) Extension of the upper lithosphere in the outer rise and seaward footwall of the trench will lead to fracturing, increasing the rock porosity, and 2) opened cracks provide pathways into the lithosphere for seawater, which will then hydrate relatively dry lower oceanic crust and upper mantle. To distinguish between these two mechanisms we would need good constraints on the shear wave velocity [*Contreras-Reyes et al.*, 2008b], which our data unfortunately do not provide (Section 3). We therefore consider both explanations in our interpretation of the compressional seismic velocity structure of transect SERP (Figure 6).

[38] The bathymetry of the EPR segment of the Cocos plate clearly shows trench-parallel faults, some as long as 50 km [*Grevemeyer et al.*, 2005], outboard of the MAT (Figure 1). The magnetic anomalies of the EPR crust are nearly parallel to the trench as well, so its abyssal hill fabric can be reactivated during plate bending [*Masson*, 1991; *McIntosh et al.*, 2007]. The swath of the seafloor that is clearly affected by bend faulting increases from southeast to northwest along the MAT, from less than 20 km offshore Nicoya Peninsula to more than 50 km offshore northwestern Nicaragua [*Ranero et al.*, 2008]. Much of this change in the seafloor faulting occurs along a ~120 km wide section of transect SERP between OBS sites OBS 9 and OBS 15 (Figure 1). The along-strike variation in the amount of brittle extension of the seafloor correlates well with the dip of the slab beneath the forearc [*Protti et al.*, 1994; *Syracuse and Abers*, 2006].

[39] In contrast to the EPR segment, there is no good indication that the seamount-studded CN crust has developed significant bending-related faults near the MAT offshore central Costa Rica (Figure 1). The shallow subduction dip angle of the Cocos plate here does not require much bending. In addition, reactivation of normal faults is not as likely on the CNS1 and CNS2 segments as on the EPR segment, because the abyssal hill fabric is not aligned well here with the bending axis [*Ranero et al.*, 2008]. Fault blocks that formed during seafloor spreading at the CN spreading center are oriented almost perpendicular to the adjacent MAT, and they appear relatively undisturbed in the trench outer wall [*von Huene et al.*, 2000]. Even if bending of the Cocos plate offshore central Costa Rica leads to faulting, transect SERP would not capture much of this process because the track line diverges from the MAT by approximately 50 km at the south end (Figure 1).

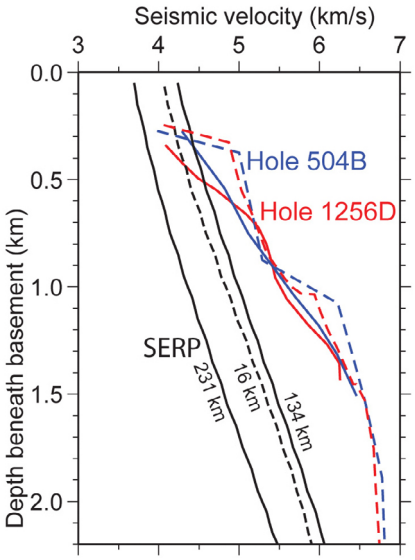

Figure 13. Comparison of three 1-D upper crustal seismic velocity profiles (black lines) from the EPR segment of our model (Figure 6) with vertical seismic profiling (VSP) and OBS refraction studies at ODP Hole 405B (blue) and IODP Hole 1256D (red). The VSP study at Hole 504B (blue solid) [*Little and Stephen*, 1985] and at Hole 1256D (red solid) [*Swift et al.*, 2008] presumably show the vertical seismic velocity gradient in the upper oceanic crust with better resolution than the coincident OBS studies of *Detrick et al.* [1998] (dashed blue) and *Expedition 309/312 Scientists* [2006] (dashed red) at these sites. The upper crustal seismic velocity at 16 km, 134 km, and 231 km in our SERP model (Figure 6) are clearly reduced compared to the structure of unaltered oceanic crust produced at the EPR.

[40] The seismic velocities that we imaged in the upper crust of the EPR segment of the Cocos plate near the MAT are relatively low for mature oceanic crust produced at a fast spreading mid-ocean ridge (Figure 13). For example, near Hole 504B, which sampled pillow basalts and a transition zone between pillows and sheeted dikes, a borehole seismic study found compressional velocities increasing from 4.0 km/s to 5.5 km/s in the top 1.0 km [*Little and Stephen*, 1985]. A similar study at Hole 1256D, which mostly drilled through lava flows in the upper crust, gave almost the same result [*Swift et al.*, 2008]. These gradients are considerably higher than what we imaged in the upper oceanic crust of the EPR segment on transect SERP (Figure 13). The difference between the seismic velocities in our model and those obtained at Hole 504B and 1256D is largest, roughly 1.2 km/s, at ~1.5 km depth beneath the basement surface. At these shallow depths, seismic velocity is controlled more by porosity than lithology [*Wilkens et al.*, 1991]. We therefore assume that plate bending induced brittle failure of the upper oceanic crust near the MAT, which then increased the macroporosity.

[41] The seismic velocity of the lower oceanic crust imaged on the EPR segment of transect SERP (Figure 6) is lower than average for mature EPR lower crust [*White et al.*, 1992]. This discrepancy in seismic velocity is on the order of 0.2–0.5 km/s, clearly less than in the upper crust on transect SERP (0.8–1.2 km/s). The downward decrease in this low-velocity anomaly is probably due to a coincident decrease in the rock porosity [*Carlson and Herrick*, 1990]. The lateral decrease in seismic velocity of the lower oceanic crust from the southeastern end of the EPR segment to northwestern end of our seismic line coincides with more pervasive faulting of the seafloor (Figure 14). This correlation suggests that crustal faults break from the surface into the lower oceanic crust near the MAT, increasing its porosity and the degree of chemical alteration.

[42] We imaged mantle seismic velocities lower than 8 km/s to depths of 18–25 km below sea level, or 7–14 km beneath the Moho, on the EPR segment of our transect (Figure 6), which is comparable to the depth of seismic reflections from normal faults imaged in the Cocos plate by *Ranero et al.* [2003] offshore southwestern Nicaragua. The low velocities here may be attributed mostly to serpentinization of the mantle rock [e.g., *Christensen*, 2004; *Grevemeyer et al.*, 2007], which suggests that hydration of the mantle was limited to the upper portion that experienced extensional faulting. We can obtain a second indication of the depth of faulting in the Cocos plate from the depth and focal mechanisms of earthquakes. Recent seismicity studies offshore Nicaragua [*Lefeldt and Grevemeyer*, 2008; *Lefeldt et al.*, 2009] indicate that the neutral plane between focal mechanisms of extensional and compressional seismic events lies at a depth of just 12 km beneath the seafloor, or 6 km beneath the Moho, which is 1 km to 8 km shallower than the depth of the 8 km/s contour in our seismic velocity model of transect SERP (Figure 6). Possibly, the resolution of tomographic inversion (Figure 9) is not sufficient to determine the precise depth of this mantle low-velocity anomaly. Alternatively, the depth discrepancy may be explained by temporal stress variations in the subducting plate between large interplate earthquakes. *Lefeldt et al.* [2009] suggest that the Cocos plate was in a coupled, compressive state when they recorded their seismicity data, and that extensional stresses may reach

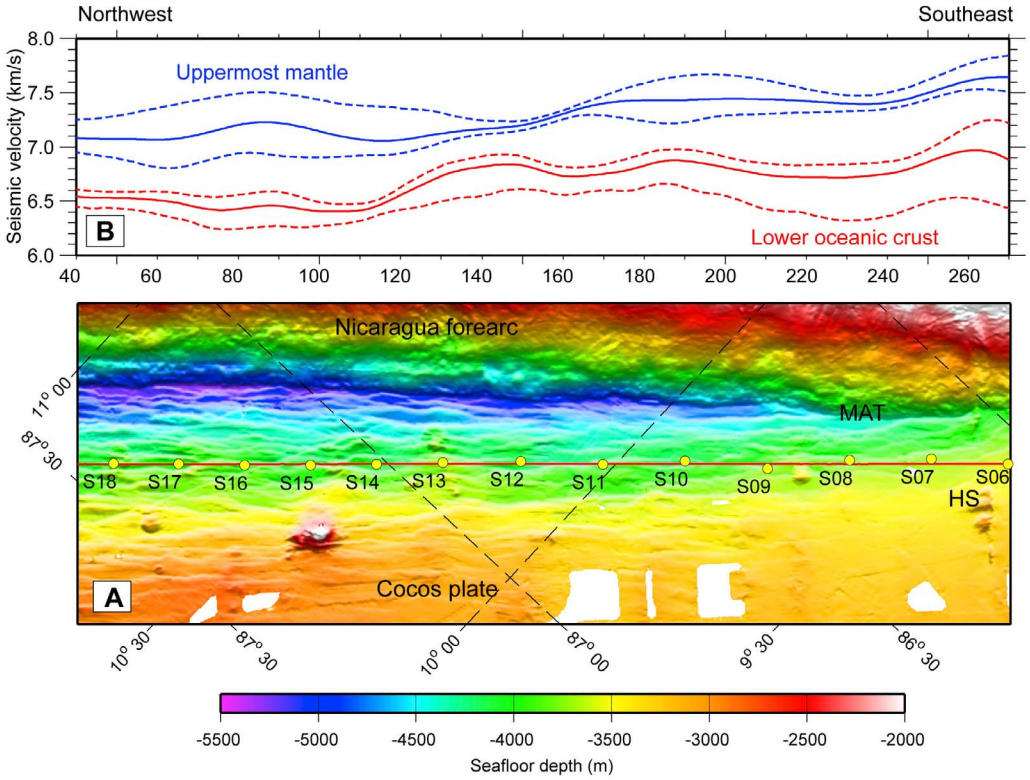

Figure 14. Comparison of seafloor relief and seismic velocities of the EPR segment. (a) Shaded bathymetry map of the MAT and a portion of transect SERP (red) with OBS locations (yellow circles). HS, Hernando Scarp. (b) Averages of seismic velocity from model SERP in the oceanic lower crust (red) and upper mantle. The solid red line represents the average velocity in the 3 km above the Moho. The dashed red lines represent the highest and lowest seismic velocity in that same depth bracket. The solid blue line is the average seismic velocity in the upper 3 km of the oceanic mantle along transect SERP. The two dashed lines are the highest and lowest seismic velocity in the top 3 km of the mantle.

deeper in the subducting slab after the stress drops during a megathrust event. We propose that normal faults in the 24 Ma old Cocos plate outboard of the trench offshore central and northwestern Nicaragua have reached to depths of 7 km to 14 km beneath the Moho over time.

5.3. Water Storage in the Cocos Slab

[43] Since the seismic velocities of the oceanic lower crust and upper mantle are affected by the degree of hydration [*Carlson*, 2003; *Christensen*, 2004], we can use our model of transect SERP (Figure 6) to estimate the flux of hydrous fluids from the deeper portions of the slab to the overlying mantle wedge and into the lower mantle. A portion of the deep water cycle comes from marine sediments and upper oceanic crust [*Rüpke et al.*, 2004; *Hacker*, 2008]. However, we cannot estimate this contribution from the seismic velocity structure of the Cocos plate near the MAT. The seismic velocity in the sediments and shallow oceanic crust is controlled more by porosity than by lithology [*Berge et al.*, 1992], so our seismic velocity model is not useful to estimate the amount of structural water (H_2O^+) that subducts beyond the forearc. Water stored in pore space and exchangeable water (H_2O^-) in clays and zeolites of the upper oceanic crust [*Staudigel et al.*, 1995] is mostly expelled beneath the accretionary prism and the outer forearc [*Silver et al.*, 2000; *Sahling et al.*, 2008]. Crystal bound H_2O^+ is more abundant in the deeper sheeted dikes (~3%) than in the shallower extrusives (~1%) at Hole 504B [*Alt et al.*, 1996], and we use these values to estimate the flux of water from the Cocos plate slab to the overlying mantle wedge in our study area.

[44] The amount of structural water of unaltered gabbroic lower crust may be as low as 0.5% by weight [*Carlson*, 2003; *Carlson and Miller*, 2004], although *Hacker et al.* [2003a] assume that alteration to about 1.3% is common. On the EPR segment of the Cocos plate, strong hydrothermal

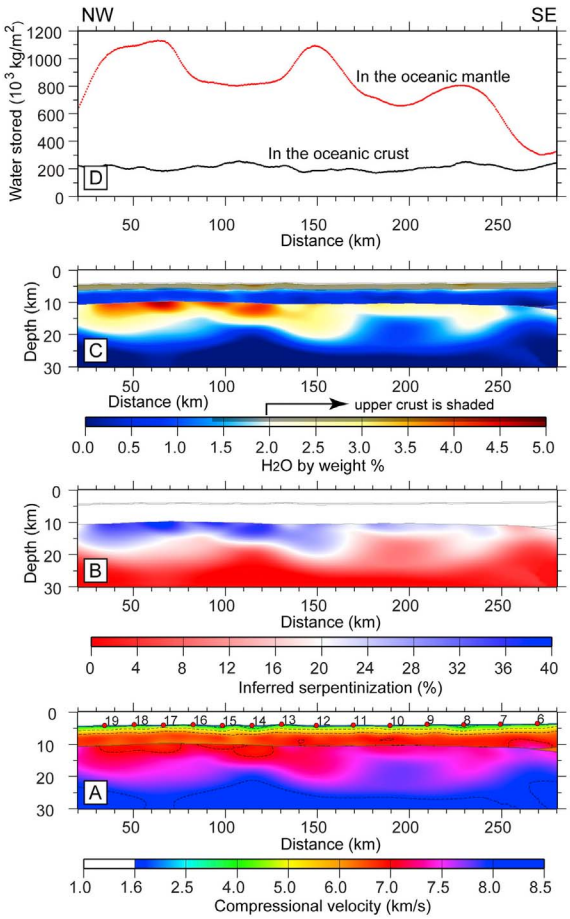

Figure 15. Estimate of structural water mass stored in the oceanic lithosphere of the Cocos plate along the EPR segment of transect SERP. (a) Detail of the final seismic velocity model of our study. (b) Estimate of the amount of serpentinization of the oceanic mantle using *Christensen*'s [2004] empirical relationship between seismic velocity and serpentinization. (c) Estimated percentage of crystal bound H_2O by weight, based on empirical relationships for the lower crust and upper mantle [*Carlson*, 2003; *Carlson and Miller*, 2003]. The upper oceanic crust is shaded because seismic velocity here is mostly controlled by porosity [*Swift et al.*, 2008], hence we do not have control on the crystal bound ($H2O^+$) water in the upper crust. (d) Estimates of chemically stored water in the subducting oceanic crust and mantle lithosphere between northwestern Nicaragua (NW) and Nicoya Peninsula (SE).

circulation far from the MAT [*Hutnak et al.*, 2008], as well as fracturing of the crust during bending near the MAT [*Grevemeyer et al.*, 2005], may have produced hydrous minerals such as chlorite and amphibole that would add substantially to the H_2O^+ inventory of the lower oceanic crust. The low heat flow near the MAT [e.g., *Harris et al.*, 2010] suggests that the temperature at the Moho has cooled to 150°C [*Harris and Wang*, 2002]. It is therefore likely that the lower crust of the EPR segment has been exposed to seawater penetrating along faults under a wide range of temperatures, which in turn resulted in different hydrothermal alteration products [*McCollom and Shock*, 1998]. To get an upper limit for the amount of water stored in hydrous minerals we apply the relationship of *Carlson* [2003], assuming that bending fractures in the lower crust are not directly responsible for the low seismic velocities. Given that seismic velocities in the lower crust along transect SERP offshore Nicaragua are as low as 6.5–6.7 km/s (Figure 14), we estimate that the water content by weight in the lower crust is around 1% (Figure 15c).

[45] Serpentinite in the mantle of the incoming plate is believed to be of major importance to the deep water cycle in subduction zones [*Rüpke et al.*, 2004]. Marine seismic refraction studies may provide the best quantitative estimates for the degree of serpentinization, although we must again consider the possibility that besides chemical alteration, mantle seismic velocity structure may also be influenced by intrinsic seismic anisotropy [*Hess*, 1964] and extensional fractures in the mantle near the trench [*Faccenda et al.*, 2008]. A seismic refraction study near the Chilean trench [*Contreras-Reyes et al.*, 2008b] showed that the Poisson's ratio in this setting is high, which indicates that serpentinization is largely responsible for the low mantle seismic velocity [*Christensen*, 2004]. A second problem in the interpretation of the deepest section of our seismic velocity model (Figure 6) is the fact that the spatial resolution of our tomographic inversion is low at depths larger than 15 km below sea level (Figure 9). The smoothness constraints that we applied in the tomographic inversion give us a spatial average of the seismic velocity structure, and the distance over which velocities are averaged will increase when the ray coverage is poor. Fortunately, we were able to image seismic velocities larger than 8 km/s at depths larger than 25 km below sea level (Figure 6), so we believe that we can estimate the amount of serpentinization in the incoming plate (Figure 15b). The boundary between altered and unaltered mantle must be sharper than our model suggests. Mantle seismic velocities lower than 7 km/s offshore central and northwestern Nicaragua indicate that the uppermost mantle is about 30% serpentinized [*Christensen*, 2004] if all of the velocity reduction is attributed to serpentization. This corresponds to an average water content of about 3.5% [*Carlson and Miller*, 2003]. Mantle seismic velocities at the southeastern edge of the EPR segment

offshore Nicoya Peninsula are much closer to 8 km/s, so they require a water content of just 1–2% in the upper 3 km of the incoming mantle (Figure 15).

[46] Despite the limitations of imaging deep seismic velocity structure of the incoming Cocos plate with OBS seismic refraction data, and the ambiguity in its interpretation, two results from our analysis of the EPR segment stand out (Figure 15d): 1) We estimate that the amount of structural water in the mantle of the subducting slab is about 2.5 times larger offshore central Nicaragua (to the northwest) than offshore Nicoya Peninsula (to the southeast). 2) In the southeast of the EPR segment, the amount of water carried by the oceanic mantle is comparable to the amount of water in the subducting oceanic crust, but to the northwest the integrated mass of structurally bound water in the mantle is potentially 4 times larger. Our seismic velocity model cannot constrain the contribution of chemically bound water in the extrusive upper oceanic crust (Figure 15c). However, if the data for altered oceanic crust at Hole 504B apply here [*Alt et al.*, 1996], we do not expect that fracturing and alteration of the oceanic crust significantly increases its H_2O input into the deeper subduction zone.

5.4. Cocos Plate Seismic Structure and Arc Geochemistry

[47] Our interpretation of the seismic velocity structure of the EPR segment of transect SERP suggests a strong variation along the Central American arc in the input of water from the oceanic mantle of the Cocos Plate (Figure 15). The depth at which H_2O is released from the slab depends on the stability of hydrous minerals and the temperature structure of the subduction zone [*Ulmer and Trommsdorff*, 1995; *Schmidt and Poli*, 1998]. A geodynamic modeling study of the subduction zone of Costa Rica and Nicaragua [*Peacock et al.*, 2005] found that mantle rock in the downgoing slab may not heat up fast enough to dehydrate. Such models are quite sensitive to the fine structure of mantle flow in the outer mantle wedge [*van Keken et al.*, 2002; *Kelemen et al.*, 2003; *Conder*, 2005], so observations such as those presented by our study help to test the assumptions on which these numerical models are based. The seismic velocity [*Syracuse et al.*, 2008] and attenuation [*Rychert et al.*, 2008] images of the mantle wedge in Costa Rica and Nicaragua provide compelling evidence for a larger discharge of hydrous fluids beneath Nicaragua compared to Costa Rica. Since seismic velocities of oceanic crust offshore Nicaragua are not dramatically reduced (Figure 14) and the water content of oceanic lower crust is normally low [*Carlson*, 2003], we expect that the large along-arc variation in mantle wedge hydration is due to the breakdown of serpentinites several kilometers beneath the Moho of the Cocos plate (Figure 15). According to laboratory data [*Ulmer and Trommsdorff*, 1995] this would require temperatures larger than 600°C in the subducting slab mantle beneath Nicaragua.

[48] As we noted in Section 2, the linear trend in Ba/La and B/La between the central Costa Rican and northwestern Nicaragua arc lavas has been attributed to a larger volume of serpentinite breakdown in the Cocos plate beneath Nicaragua [*Rüpke et al.*, 2002] or an enrichment of incompatible elements in the mantle beneath central Costa Rica [*Carr et al.*, 2007]. The results of our study are consistent with both models to some degree. Our seismic velocity model suggests that the mantle of the Cocos plate offshore central and northwestern Nicaragua carries about 2.5 times more water than offshore Nicoya Peninsula (Figure 15), which correlates very well with the trend in Ba/La and B/La ratios of arc lavas [*Carr et al.*, 2003]. However, the Ba/La ratio decreases farther to the southwest from 43 to 47 in northwestern Costa Rica to 17–23 in central Costa Rica (Figure 1). The EPR mantle subducting beneath Nicoya Peninsula can only be lightly hydrated, because the sub-Moho seismic velocities in our model here (at 220 km in Figure 6) approach 8 km/s. It is therefore plausible that the decrease in Ba/La and B/La between northwestern Costa Rica and central Costa Rica is due to OIB enrichment [*Gazel et al.*, 2009]. The thick oceanic crust of the CNS1 and CNS2 segments (Figure 6) indicates that the Galápagos hot spot has influenced the composition of the Cocos plate up to the FB discontinuity (Figure 1), which can explain the very low Ba/La values in central Costa Rica (Figure 1).

6. Conclusions

[49] We acquired and analyzed OBS seismic refraction data along the 396 km long transect SERP on the Cocos plate parallel to the MAT to image variations in crustal and upper mantle structure of the subducting lithosphere between central Costa Rica and northwestern Nicaragua. Our seismic velocity model shows a distinct difference between oceanic crust produced at the EPR and CN spreading centers. We also use this seismic velocity model to estimate the effect of bend faulting on the deep structure of the Cocos plate near the MAT. We can draw the following conclusions:

[50] 1. The crustal seismic velocity structure of the CNS1 and CNS2 spreading segments is much more complex than the structure of the crust produced at the EPR. The CN crust is 8–11 km thick, with intracrustal seismic reflections and seismic velocities that are lower than normal for oceanic crust. Our seismic reflection and refraction tomographic inversion (Figure 6) even shows evidence for a low-velocity (~6.3 km/s) lower crust in the vicinity of the Farallon breakup (FB) trace. The anomalous seismic structure at the southeastern portion of transect SERP may be a record of the igneous processes in the early history of the CN spreading center and subsequent interaction with the Galápagos hot spot. The EPR crust that formed near the trench 24 Ma ago is normal 6 km thick oceanic crust, typical of fast spreading mid-ocean ridges.

[51] 2. The mantle seismic velocities beneath the EPR segment of the SERP transect decrease to the northwest from ~7.8 km/s near the FB discontinuity to less than 7.0 km/s offshore central and northwestern Nicaragua. This seismic velocity trend correlates well with the degree of faulting on the seafloor (Figure 14), which gives more evidence that the mantle lithosphere of the Cocos plate subducting beneath Nicaragua is more serpentinized than the Cocos plate offshore Costa Rica. Our estimate of the water content of the downgoing oceanic mantle indicates that the water intake offshore central Nicaragua is about 2.5 times larger than offshore Nicoya Peninsula (Figure 15). In contrast, we do not expect that the oceanic crust of the Cocos plate offshore Nicaragua is significantly more hydrated than elsewhere along the MAT.

[52] 3. The contrasts in crustal and mantle structure along transect SERP help to explain the geochemical trends along the Central American arc. The apparent influence of the Galápagos hot spot on the Cocos plate southeast of the FB discontinuity may be responsible for the low Ba/La ratios in central Costa Rica compared to Nicoya Peninsula. Farther to the northwest, we infer a gradual increase in the hydration of the Cocos plate mantle. The discharge of larger amounts of hydrous fluids beneath central and northwestern Nicaragua may explain the large abundance of fluid mobile elements in Nicaragua arc lavas.

Acknowledgments

[53] We gratefully thank the officers and crew of the R/V *Marcus Langseth* and the R/V *New Horizon* and the engineers and technicians of the U.S. OBS Instrument Pool for their hard work during the TICOCAVA project. We thank Ingo Grevemeyer, Nick Hayman, Luc Lavier, and an anonymous reviewer for useful comments and discussions. This work was funded by the U.S. National Science Foundation MARGINS program under grants OCE0405556, OCE 0405654, and OCE 0625178. This is UTIG contribution 2376.

References

Abers, G. A., T. Plank, and B. R. Hacker (2003), The wet Nicaraguan slab, *Geophys. Res. Lett.*, *30*(2), 1098, doi:10.1029/2002GL015649.

Alt, J. C., et al. (1996), Hydrothermal alteration of a section of upper oceanic crust in the eastern equatorial Pacific: A synthesis of results from Site 504 (DSDP Legs 69, 70, and 83, and ODP Legs 111, 137, 140, and 148), *Proc. Ocean Drill. Program Sci. Results*, *148*, doi:10.2973/odp.proc.sr.148.159.1996.

Barckhausen, U., C. R. Ranero, R. von Huene, S. C. Cande, and H. A. Roeser (2001), Revised tectonic boundaries in the Cocos plate off Costa Rica: Implications for the segmentation of the convergent margin and for plate tectonic models, *J. Geophys. Res.*, *106*, 19,207–19,220, doi:10.1029/2001JB000238.

Barckhausen, U., C. R. Ranero, S. C. Cande, M. Engels, and W. Weinrebe (2008), Birth of an intraoceanic spreading center, *Geology*, *36*, 767–770, doi:10.1130/G25056A.1.

Berge, P. A., G. J. Fryer, and R. H. Wilkens (1992), Velocity-porosity relationships in the upper oceanic crust: Theoretical considerations, *J. Geophys. Res.*, *97*, 15,239–15,254.

Bolge, L. L., M. J. Carr, K. I. Milidakis, F. N. Lindsay, and M. D. Feigenson (2009), Correlating geochemistry, tectonics, and volcanic volume along the Central American volcanic front, *Geochem. Geophys. Geosyst.*, *10*, Q12S18, doi:10.1029/2009GC002704.

Caldwell, J. G., W. F. Haxby, D. E. Karig, and D. L. Turcotte (1976), Applicability of a universal elastic trench profile, *Earth Planet. Sci. Lett.*, *31*, 239–246, doi:10.1016/0012-821X(76)90215-6.

Canales, J. P., G. Ito, R. S. Detrick, and J. Sinton (2002), Crustal thickness along the western Galapagos spreading center and the compensation of the Galapagos hotspot swell, *Earth Planet. Sci. Lett.*, *203*, 311–327, doi:10.1016/S0012-821X(02)00843-9.

Cardace, D., and J. D. Morris (2009), Geochemical evidence for sediment accretion in the Costa Rica frontal prism, *Geology*, *37*, 891–894, doi:10.1130/G25631A.1.

Carlson, R. L. (2003), Bound water content of the lower oceanic crust estimated from modal analyses and seismic velocities of oceanic diabase and gabbro, *Geophys. Res. Lett.*, *30*(22), 2142, doi:10.1029/2003GL018213.

Carlson, R. L., and C. N. Herrick (1990), Densities and porosities in the oceanic crust and their variations with depth and age, *J. Geophys. Res.*, *95*, 9153–9170, doi:10.1029/JB095iB06p09153.

Carlson, R. L., and D. J. Miller (2003), Mantle wedge water contents estimated from seismic velocities in partially serpentinized peridotites, *Geophys. Res. Lett.*, *30*(5), 1250, doi:10.1029/2002GL016600.

Carlson, R. L., and D. J. Miller (2004), Influence of pressure and mineralogy on seismic velocities in oceanic gabbros: Implications for the composition and state of the lower oceanic crust, *J. Geophys. Res.*, *109*, B09205, doi:10.1029/2003JB002699.

Carr, M. J., M. D. Feigenson, and E. A. Bennett (1990), Incompatible element and isotopic evidence for tectonic control of source mixing and melt extraction along the Central American arc, *Contrib. Mineral. Petrol.*, *105*, 369–380, doi:10.1007/BF00286825.

Carr, M. J., M. D. Feigenson, L. C. Patino, and J. A. Walker (2003), Volcanism and geochemistry in central America: Progress and problems, in *Inside the Subduction Factory*, *Geophys. Monogr. Ser.*, vol. 138, edited by J. Eiler, pp. 153–174, AGU, Washington, D. C.

Carr, M. J., I. Saginor, G. E. Alvarado, L. L. Bolge, F. N. Lindsay, K. Milidakis, B. D. Turrin, M. D. Feigenson, and C. C. Swisher III (2007), Element fluxes from the volcanic front of Nicaragua and Costa Rica, *Geochem. Geophys. Geosyst.*, *8*, Q06001, doi:10.1029/2006GC001396.

Chapple, W. M., and D. W. Forsyth (1979), Earthquakes and bending of plates at trenches, *J. Geophys. Res.*, *84*, 6729–6749, doi:10.1029/JB084iB12p06729.

Christensen, N. I. (2004), Serpentinites, peridotites, and seismology, *Int. Geol. Rev.*, *46*, 795–816, doi:10.2747/0020-6814.46.9.795.

Christeson, G. L., Y. Nakamura, K. D. McIntosh, and P. L. Stoffa (1996), Effect of shot interval on ocean bottom seismograph and hydrophone data, *Geophys. Res. Lett.*, *23*, 3783–3786, doi:10.1029/96GL03572.

Christeson, G. L., K. D. McIntosh, T. H. Shipley, E. R. Flueh, and H. Goedde (1999), Structure of the Costa Rica convergent margin, offshore Nicoya Peninsula, *J. Geophys. Res.*, *104*, 25,443–25,468, doi:10.1029/1999JB900251.

Conder, J. A. (2005), A case for hot slab surface temperatures in numerical viscous flow models of subduction zones with an improved fault zone parameterization, *Phys. Earth Planet. Inter.*, *149*, 155–164, doi:10.1016/j.pepi.2004.08.018.

Contreras-Reyes, E., I. Grevemeyer, E. R. Flueh, and C. Reichert (2008a), Upper lithospheric structure of the subduction zone offshore of southern Arauco peninsula, Chile, at ~38°S, *J. Geophys. Res.*, *113*, B07303, doi:10.1029/2007JB005569.

Contreras-Reyes, E., I. Grevemeyer, E. R. Flueh, M. Scherwath, and J. Bialas (2008b), Effect of trench-outer rise bending-related faulting on seismic Poisson's ratio and mantle anisotropy: A case study offshore of southern central Chile, *Geophys. J. Int.*, *173*, 142–156, doi:10.1111/j.1365-246X.2008.03716.x.

Coulbourn, W. T., R. Hesse, J. Azema, and T. Shiki (1982), A summary of sedimentology of DSDP Leg 67 sites: The Middle America trench and slope off Guatamala–an active margiun transect, *Deep Sea Drill. Program, Initial Rep.*, *67*, 759–774, doi:10.2973/dsdp.proc.67.142.1982.

Davis, D., J. Suppe, and F. Dahlen (1983), Mechanics of fold-and-thrust belts and accretionary wedges, *J. Geophys. Res.*, *88*, 1153–1172.

Detrick, R., D. Toomey, and J. Collins (1998), Three-dimensional upper crustal heterogeneity and anisotropy around Hole 504B from seismic tomography, *J. Geophys. Res.*, *103*, 30,485–30,504.

Eiler, J. M., M. J. Carr, M. Reagan, and E. Stolper (2005), Oxygen isotope constraints on the sources of Central American lavas, *Geochem. Geophys. Geosyst.*, *6*, Q07007, doi:10.1029/2004GC000804.

Escartín, J., G. Hirth, and B. Evans (2001), Strength of slightly serpentinized peridotites: Implications for the tectonics of oceanic lithosphere, *Geology*, *29*, 1023–1026, doi:10.1130/0091-7613(2001)029<1023:SOSSPI>2.0.CO;2.

Expedition 309/312 Scientists (2006), Site 1256, *Proc. Integrated Ocean Drill. Program*, *309/312*, 1–549.

Faccenda, M., L. Burlini, T. V. Gerya, and D. Mainprice (2008), Fault-induced seismic anisotropy by hydration in subducting oceanic plates, *Nature*, *455*, 1097–1100, doi:10.1038/nature07376.

Faccenda, M., T. V. Gerya, and L. Burlini (2009), Deep slab hydration induced by bending-related variations in tectonic pressure, *Nat. Geosci.*, *2*, 790–793, doi:10.1038/ngeo656.

Feigenson, M. D., M. J. Carr, S. V. Maharaj, S. Juliano, and L. L. Bolge (2004), Lead isotope composition of Central American volcanoes: Influence of the Galapagos plume, *Geochem. Geophys. Geosyst.*, *5*, Q06001, doi:10.1029/2003GC000621.

Gazel, E., M. J. Carr, K. Hoernle, M. D. Feigenson, D. Szymanski, F. Hauff, and P. van den Bogaard (2009), Galapagos-OIB signature in southern Central America: Mantle refertilization by arc–hot spot interaction, *Geochem. Geophys. Geosyst.*, *10*, Q02S11, doi:10.1029/2008GC002246.

Gazel, E., K. Hoernle, M. J. Carr, C. Herzberg, I. Saginor, P. d. Bogaard, F. Hauff, M. Feigenson, and C. Swisher (2011), Plume–subduction interaction in southern Central America: Mantle upwelling and slab melting, *Lithos*, *121*, 117–134, doi:10.1016/j.lithos.2010.10.008.

Grevemeyer, I., N. Kaul, J. L. Diaz-Naveas, H. W. Villinger, C. R. Ranero, and C. Reichert (2005), Heat flow and bending-related faulting at subduction trenches: Case studies offshore Nicaragua and central Chile, *Earth Planet. Sci. Lett.*, *236*, 238–248, doi:10.1016/j.epsl.2005.04.048.

Grevemeyer, I., C. R. Ranero, E. R. Flueh, D. Kläschen, and J. Bialas (2007), Passive and active seismological study of bending-related faulting and mantle serpentinization at the Middle America trench, *Earth Planet. Sci. Lett.*, *258*, 528–542, doi:10.1016/j.epsl.2007.04.013.

Hacker, B. R. (2008), H_2O subduction beyond arcs, *Geochem. Geophys. Geosyst.*, *9*, Q03001, doi:10.1029/2007GC001707.

Hacker, B. R., G. A. Abers, and S. M. Peacock (2003a), Subduction factory: 1. Theoretical mineralogy, densities, seismic wave speeds, and H_2O contents, *J. Geophys. Res.*, *108*(B1), 2029, doi:10.1029/2001JB001127.

Hacker, B. R., S. M. Peacock, G. A. Abers, and S. D. Holloway (2003b), Subduction factory: 2. Are intermediate-depth earthquakes in subducting slabs linked to metamorphic dehydration reactions?, *J. Geophys. Res.*, *108*(B1), 2030, doi:10.1029/2001JB001129.

Harris, R. N., and K. Wang (2002), Thermal models of the Middle America Trench at the Nicoya Peninsula, Costa Rica, *Geophys. Res. Lett.*, *29*(21), 2010, doi:10.1029/2002GL015406.

Harris, R. N., G. Spinelli, C. R. Ranero, I. Grevemeyer, H. Villinger, and U. Barckhausen (2010), Thermal regime of the Costa Rican convergent margin: 2. Thermal models of the shallow Middle America subduction zone offshore Costa Rica, *Geochem. Geophys. Geosyst.*, *11*, Q12S29, doi:10.1029/2010GC003273.

Herrstrom, E. A., M. K. Reagan, and J. D. Morris (1995), Variations in lava composition associated with flow of asthenosphere beneath southern Central America, *Geology*, *23*, 617–620, doi:10.1130/0091-7613(1995)023<0617:VILCAW>2.3.CO;2.

Hess, H. H. (1964), Seismic anisotropy of the uppermost mantle under oceans, *Nature*, *203*, 629–631, doi:10.1038/203629a0.

Hey, R. (1977), Tectonic evolution of the Cocos-Nazca spreading center, *Geol. Soc. Am. Bull.*, *88*, 1404–1420, doi:10.1130/0016-7606(1977)88<1404:TEOTCS>2.0.CO;2.

Hoernle, K., R. Werner, J. Phipps Morgan, D. Garbe-Schönberg, J. Bryce, and J. Mrazek (2000), Existence of complex spatial zonation in the Galápagos plume, *Geology*, *28*, 435–438, doi:10.1130/0091-7613(2000)28<435:EOCSZI>2.0.CO;2.

Hoernle, K., et al. (2008), Arc-parallel flow in the mantle wedge beneath Costa Rica and Nicaragua, *Nature*, *451*, 1094–1097, doi:10.1038/nature06550.

Hutnak, M., A. T. Fisher, R. Harris, C. Stein, K. Wang, G. Spinelli, M. Schindler, H. Villinger, and E. Silver (2008), Large heat and fluid fluxes driven through mid-plate outcrops on ocean crust, *Nat. Geosci.*, *1*, 611–614, doi:10.1038/ngeo264.

Ivandic, M., I. Grevemeyer, A. Berhorst, E. R. Flueh, and K. McIntosh (2008), Impact of bending related faulting on the seismic properties of the incoming oceanic plate offshore of Nicaragua, *J. Geophys. Res.*, *113*, B05410, doi:10.1029/2007JB005291.

Ivandic, M., I. Grevemeyer, J. Bialas, and C. J. Petersen (2010), Serpentinization in the trench-outer rise region offshore of Nicaragua: Constraints from seismic refraction and wide-angle data, *Geophys. J. Int.*, *180*, 1253–1264, doi:10.1111/j.1365-246X.2009.04474.x.

Janoušek, V., V. Erban, F. V. Holub, T. Magna, H. Bellon, B. Mlčoch, U. Wiechert, and V. Rapprich (2010), Geochemistry and genesis of behind-arc basaltic lavas from eastern Nicaragua, *J. Volcanol. Geotherm. Res.*, *192*, 232–256, doi:10.1016/j.jvolgeores.2010.02.023.

Kelemen, P. B., J. L. Rilling, E. M. Parmentier, L. Mehl, and B. R. Hacker (2003), Thermal structure due to solid-state flow in the mantle wedge beneath arcs, in *Inside the Subduction Factory*, *Geophys. Monogr. Ser.*, vol. 138, edited by J. Eiler, pp. 293–311, AGU, Washington, D. C.

Kelly, R. K. (2003), Subduction dynamics at the Middle America Trench: New constraints from swath bathymetry, multichannel seismic data, and 10Be, Ph.D. thesis, 334 pp., Woods Hole Joint Program, Mass. Inst. of Technol., Boston.

Koepke, J., J. Berndt, S. T. Feig, and F. Holtz (2007), The formation of SiO_2-rich melts within the deep oceanic crust by hydrous partial melting of gabbros, *Contrib. Mineral. Petrol.*, *153*, 67–84, doi:10.1007/s00410-006-0135-y.

Langseth, M. G., and E. A. Silver (1996), The Nicoya convergent margin: A region of exceptionally low heat flow, *Geophys. Res. Lett.*, *23*, 891–894, doi:10.1029/96GL00733.

Leeman, W. P., M. J. Carr, and J. D. Morris (1994), Boron geochemistry of the Central American volcanic arc: Constraints on the genesis of subduction-related magmas, *Geochim. Cosmochim. Acta*, *58*, 149–168, doi:10.1016/0016-7037(94)90453-7.

Lefeldt, M., and I. Grevemeyer (2008), Centroid depth and mechanism of trench-outer rise earthquakes, *Geophys. J. Int.*, *172*, 240–251, doi:10.1111/j.1365-246X.2007.03616.x.

Lefeldt, M., I. Grevemeyer, J. Goßler, and J. Bialas (2009), Intraplate seismicity and related mantle hydration at the Nicaraguan trench outer rise, *Geophys. J. Int.*, *178*, 742–752, doi:10.1111/j.1365-246X.2009.04167.x.

Little, S. A., and R. A. Stephen (1985), Costa Rica Rift borehole seismic experiment, Deep Sea Drilling Project Hole 504B, Leg 92, *Deep Sea Drill. Project Initial Rep.*, *83*, 517–528, doi:10.2973/dsdp.proc.83.129.1985.

Lizarralde, D., J. B. Gaherty, J. A. Collins, G. Hirth, and S. D. Kim (2004), Spreading-rate dependence of melt extraction at mid-ocean ridges from mantle seismic refraction data, *Nature*, *432*, 744–747, doi:10.1038/nature03140.

Lonsdale, P. (2005), Creation of the Cocos and Nazca plates by fission of the Farallon plate, *Tectonophysics*, *404*, 237–264, doi:10.1016/j.tecto.2005.05.011.

Masson, D. G. (1991), Fault patterns at outer trench walls, *Mar. Geophys. Res.*, *13*, 209–225, doi:10.1007/BF00369150.

McCollom, T., and E. Shock (1998), Fluid-rock interactions in the lower oceanic crust: Thermodynamic models of hydrothermal alteration, *J. Geophys. Res.*, *103*, 547–575, doi:10.1029/97JB02603.

McIntosh, K. D., E. A. Silver, I. Ahmed, A. Berhorst, C. R. Ranero, R. K. Kelly, and E. R. Flueh (2007), The Nicaragua convergent margin: Seismic reflection imaging of the source of a tsunami earthquake, in *The Seismogenic Zone of Subduction Thrust Faults*, edited by T. Dixon and J. C. Moore, pp. 257–287, Columbia Univ. Press, New York.

McNutt, M. K., and H. W. Menard (1982), Constraints on yield strength in the oceanic lithosphere derived from observations of flexure, *Geophys. J. R. Astron. Soc.*, *71*, 363–394.

Menke, W. (1984), *Geophysical Data Analysis: Discrete Inverse Theory*, 289 pp., Academic, San Diego, Calif.

Meschede, M., U. Barckhausen, and H.-U. Worm (1998), Extinct spreading on the Cocos Ridge, *Terra Nova*, *10*, 211–216, doi:10.1046/j.1365-3121.1998.00195.x.

Moore, J. C., and D. Saffer (2001), Updip limit of the seismogenic zone beneath the accretionary prism of southwest Japan: An effect of diagenetic to low-grade metamorphic processes and increasing effective stress, *Geology*, *29*, 183–186, doi:10.1130/0091-7613(2001)029<0183:ULOTSZ>2.0.CO;2.

Morris, J. D., and S. R. Hart (1983), Isotopic and incompatible element constraints on the genesis of island arc volcanics from Cold Bay and Amak Island, Aleutians, and implications for mantle structure, *Geochim. Cosmochim. Acta*, *47*, 2015–2030.

Morris, J. D., W. P. Leeman, and F. Tera (1990), The subducted component in island arc lavas: Constraints from Be isotopes and B–Be systematics, *Nature*, *344*, 31–36, doi:10.1038/344031a0.

Moser, T. J. (1991), Shortest path calculation of seismic rays, *Geophysics*, *56*, 59–67, doi:10.1190/1.1442958.

Moser, T. J., G. Nolet, and R. K. Snieder (1992), Ray bending revisited, *Bull. Seismol. Soc. Am.*, *82*, 259–288.

Noll, P. D., H. E. Newsom, W. P. Leeman, and J. G. Ryan (1996), The role of hydrothermal fluids in the production of subduction zone magmas: Evidence from siderophile and chalcophile trace elements and boron, *Geochim. Cosmochim. Acta*, *60*, 587–611, doi:10.1016/0016-7037(95)00405-X.

Patino, L. C., M. J. Carr, and M. D. Feigenson (2000), Local and regional variations in central American arc lavas controlled by variations in subducted sediment input, *Contrib. Mineral. Petrol.*, *138*, 265–283, doi:10.1007/s004100050562.

Peacock, S. M., P. E. Van Keken, S. D. Holloway, B. R. Hacker, G. A. Abers, and R. L. Fergason (2005), Thermal structure of the Costa Rica-Nicaragua subduction zone, *Phys. Earth Planet. Inter.*, *149*, 187–200, doi:10.1016/j.pepi.2004.08.030.

Plank, T., and C. H. Langmuir (1998), The chemical composition of subducting sediment and its consequences for the crust and mantle, *Chem. Geol.*, *145*, 325–394, doi:10.1016/S0009-2541(97)00150-2.

Protti, M., F. Gundel, and K. McNally (1994), The geometry of the Wadati-Benioff zone under southern Central America and its tectonic significance: Results from a high-resolution local seismographic network, *Phys. Earth Planet. Inter.*, *84*, 271–287, doi:10.1016/0031-9201(94)90046-9.

Ranero, C. R., and V. Sallarès (2004), Geophysical evidence for hydration of the crust and mantle of the Nazca plate dur-

ing bending at the north Chile Trench, *Geology*, *32*, 549–552, doi:10.1130/G20379.1.

Ranero, C. R., J. Phipps Morgan, K. McIntosh, and C. Reichert (2003), Bending-related faulting and mantle serpentinization at the Middle America Trench, *Nature*, *425*, 367–373, doi:10.1038/nature01961.

Ranero, C. R., A. Villaseñor, J. Phipps Morgan, and W. Weinrebe (2005), Relationship between bend-faulting at trenches and intermediate-depth seismicity, *Geochem. Geophys. Geosyst.*, *6*, Q12002, doi:10.1029/2005GC000997.

Ranero, C. R., I. Grevemeyer, H. Sahling, U. Barckhausen, C. Hensen, K. Wallmann, W. Weinrebe, P. Vannucchi, R. von Huene, and K. McIntosh (2008), Hydrogeological system of erosional convergent margins and its influence on tectonics and interplate seismogenesis, *Geochem. Geophys. Geosyst.*, *9*, Q03S04, doi:10.1029/2007GC001679.

Rüpke, L. H., J. Phipps Morgan, M. Hort, and J. A. D. Connoly (2002), Are the regional variations in Central America arc lavas due to differing basaltic versus peridotitic slab sources or fluids?, *Geology*, *30*, 1035–1038, doi:10.1130/0091-7613(2002)030<1035:ATRVIC>2.0.CO;2.

Rüpke, L. H., J. Phipps Morgan, M. Hort, and J. A. D. Connolly (2004), Serpentine and the subduction zone water cycle, *Earth Planet. Sci. Lett.*, *223*, 17–34, doi:10.1016/j.epsl.2004.04.018.

Rychert, C. A., K. M. Fischer, G. A. Abers, T. Plank, E. M. Syracuse, J. M. Protti, V. Gonzalez, and W. Strauch (2008), Strong along-arc variations in attenuation in the mantle wedge beneath Costa Rica and Nicaragua, *Geochem. Geophys. Geosyst.*, *9*, Q10S10, doi:10.1029/2008GC002040.

Sadofsky, S. J., M. Portnyagin, K. Hoernle, and P. van den Bogaard (2008), Subduction cycling of volatiles and trace elements through the Central American volcanic arc: Evidence from melt inclusions, *Contrib. Mineral. Petrol.*, *155*, 433–456, doi:10.1007/s00410-007-0251-3.

Sadofsky, S., K. Hoernle, S. Duggen, F. Hauff, R. Werner, and D. Garbe-Schönberg (2009), Geochemical variations in the Cocos Plate subducting beneath Central America: Implications for the composition of arc volcanism and the extent of the Galápagos Hotspot influence on the Cocos oceanic crust, *Int. J. Earth Sci.*, *98*, 901–913, doi:10.1007/s00531-007-0289-5.

Sahling, H., D. G. Masson, C. R. Ranero, V. Hühnerbach, W. Weinrebe, I. Klaucke, D. Bürk, W. Brückmann, and E. Suess (2008), Fluid seepage at the continental margin offshore Costa Rica and southern Nicaragua, *Geochem. Geophys. Geosyst.*, *9*, Q05S05, doi:10.1029/2008GC001978.

Sallarès, V., and P. Charvis (2003), Crustal thickness constraints on the geodynamic evolution of the Galapagos Volcanic Province, *Earth Planet. Sci. Lett.*, *214*, 545–559, doi:10.1016/S0012-821X(03)00373-X.

Sallarès, V., J. J. Dañobeitia, and E. R. Flueh (2001), Lithospheric structure of the Costa Rican Isthmus: Effects of subduction zone magmatism on an oceanic plateau, *J. Geophys. Res.*, *106*, 621–643, doi:10.1029/2000JB900245.

Sallarès, V., P. Charvis, E. R. Flueh, and J. Bialas (2003), Seismic structure of Cocos and Malpelo volcanic Ridges and implications for hot spot-ridge interaction, *J. Geophys. Res.*, *108*(B12), 2564, doi:10.1029/2003JB002431.

Schmidt, M. W., and S. Poli (1998), Experimentally based water budgets for dehydrating slabs and consequences for arc magma generation, *Earth Planet. Sci. Lett.*, *163*, 361–379, doi:10.1016/S0012-821X(98)00142-3.

Schutt, D. L., and C. E. Lesher (2006), Effects of melt depletion on the density and seismic velocity of garnet and spinel lherzolite, *J. Geophys. Res.*, *111*, B05401, doi:10.1029/2003JB002950.

Shipboard Scientific Party (1979), Site 495: Cocos Plate - Middle American Trench outer slope, *Deep Sea Drill. Program Initial. Rep.*, *67*, 76–141.

Shipboard Scientific Party (1998), Site 1039, in *Costa Rica Accretionary Wedge*, edited by G. Kimura, E. Silver, and P. Blum, *Proc. Ocean Drill. Program Initial Rep.*, *170*, 45–93.

Shipley, T., and G. Moore (1986), Sediment accretion, subduction, and dewatering at the base of the trench slope off Costa Rica: A seismic reflection view of the décollement, *J. Geophys. Res.*, *91*, 2019–2028, doi:10.1029/JB091iB02p02019.

Silver, E., M. Kastner, A. Fisher, J. Morris, K. McIntosh, and D. Saffer (2000), Fluid flow paths in the Middle America Trench and Costa Rica margin, *Geology*, *28*, 679–682, doi:10.1130/0091-7613(2000)28<679:FFPITM>2.0.CO;2.

Staudigel, H., G. R. Davies, S. R. Hart, K. M. Marchant, and B. M. Smith (1995), Large-scale isotopic Sr, Nd, and O isotopic anatomy of altered oceanic crust - DSDP/ODP Sites 417/418, *Earth Planet. Sci. Lett.*, *130*, 169–185, doi:10.1016/0012-821X(94)00263-X.

Stolper, E., and S. Newman (1994), The role of water in the petrogenesis of Mariana Trough magmas, *Earth Planet. Sci. Lett.*, *121*, 293–325, doi:10.1016/0012-821X(94)90074-4.

Swift, S., M. Reichow, A. Tikku, M. Tominaga, and L. Gilbert (2008), Velocity structure of upper ocean crust at Ocean Drilling Program Site 1256, *Geochem. Geophys. Geosyst.*, *9*, Q10O13, doi:10.1029/2008GC002188.

Syracuse, E. M., and G. A. Abers (2006), Global compilation of variations in slab depth beneath arc volcanoes and implications, *Geochem. Geophys. Geosyst.*, *7*, Q05017, doi:10.1029/2005GC001045.

Syracuse, E. M., G. A. Abers, K. Fischer, L. MacKenzie, C. Rychert, M. Protti, V. González, and W. Strauch (2008), Seismic tomography and earthquake locations in the Nicaraguan and Costa Rican upper mantle, *Geochem. Geophys. Geosyst.*, *9*, Q07S08, doi:10.1029/2008GC001963.

Tenthorey, E., and J. Hermann (2004), Composition of fluids during serpentinite breakdown in subduction zones: Evidence for limited boron mobility, *Geology*, *32*, 865–868, doi:10.1130/G20610.1.

Tera, F., L. Brown, J. Morris, I. S. Sacks, J. Klein, and R. Middleton (1986), Sediment incorporation in island-arc magmas: Inferences from ^{10}Be, *Geochim. Cosmochim. Acta*, *50*, 535–550, doi:10.1016/0016-7037(86)90103-1.

Toomey, D. R., and G. R. Foulger (1989), Tomographic inversion of local earthquake data from the Hengill-Grensdalur central volcano complex, Iceland, *J. Geophys. Res.*, *94*, 17,497–17,510.

Ulmer, P., and V. Trommsdorff (1995), Serpentine stability to mantle depths and subduction-related magmatism, *Science*, *268*, 858–861, doi:10.1126/science.268.5212.858.

Van Avendonk, H. J. A., A. J. Harding, J. A. Orcutt, and J. S. McClain (1998), A two-dimensional tomographic study of the Clipperton transform fault, *J. Geophys. Res.*, *103*, 17,885–17,899, doi:10.1029/98JB00904.

Van Avendonk, H. J. A., A. J. Harding, J. A. Orcutt, and W. S. Holbrook (2001), Hybrid shortest path and ray bending method for traveltime and raypath calculations, *Geophysics*, *66*, 648–653, doi:10.1190/1.1444955.

Van Avendonk, H. J. A., D. J. Shillington, W. S. Holbrook, and M. J. Hornbach (2004), Inferring crustal structure in

the Aleutian arc from a sparse wide-angle seismic data set, *Geochem. Geophys. Geosyst.*, *5*, Q08008, doi:10.1029/2003GC000664.

Van Avendonk, H. J. A., W. S. Holbrook, D. Lizarralde, M. M. Mora, S. Harder, A. D. Bullock, G. E. Alvarado, and C. J. Ramírez (2010), Seismic evidence for fluids in fault zones on top of the subducting Cocos plate beneath Costa Rica, *Geophys. J. Int.*, *181*, 997–1016, doi:10.1111/j.1365-246X.2010.04552.x.

van Keken, P. E., B. Kiefer, and S. M. Peacock (2002), High-resolution models of subduction zones: Implications for mineral dehydration reactions and the transport of water into the deep mantle, *Geochem. Geophys. Geosyst.*, *3*(10), 1056, doi:10.1029/2001GC000256.

van Keken, P. E., B. R. Hacker, E. M. Syracuse, and G. A. Abers (2011), Subduction factory: 4. Depth-dependent flux of H2O from subducting slabs worldwide, *J. Geophys. Res.*, *116*, B01401, doi:10.1029/2010JB007922.

von Huene, R., C. R. Ranero, W. Weinrebe, and K. Hinz (2000), Quarternary convergent margin tectonics of Costa Rica, segmentation of the Cocos plate, and Central American volcanism, *Tectonics*, *19*, 314–334, doi:10.1029/1999TC001143.

Wade, J. A., T. Plank, W. G. Melson, and G. J. Soto (2006), The volatile content of magmas from Arenal volcano, Costa Rica, *J. Volcanol. Geotherm. Res.*, *157*, 94–120, doi:10.1016/j.jvolgeores.2006.03.045.

Walther, C. H. E. (2003), The crustal structure of the Cocos Ridge off Costa Rica, *J. Geophys. Res.*, *108*(B3), 2136, doi:10.1029/2001JB000888.

Walther, C., and E. Flueh (2002), Remnant of the ancient Farallon Plate breakup: A low-velocity body in the lower oceanic crust off Nicoya Peninsula, Costa Rica - evidence from wide-angle seismics, *Geophys. Res. Lett.*, *29*(19), 1939, doi:10.1029/2002GL015026.

Walther, C. H. E., E. Flueh, C. R. Ranero, R. von Huene, and W. Strauch (2000), Crustal structure across the Pacific margin of Nicaragua: Evidence for ophiolitic basement and a shallow mantle sliver, *Geophys. J. Int.*, *141*, 759–777, doi:10.1046/j.1365-246x.2000.00134.x.

Werner, R., K. Hoernle, P. d. Bogaard, C. Ranero, R. v. Huene, and D. Korich (1999), Drowned 14-m.y.-old Galápagos archipelago off the coast of Costa Rica: Implications for tectonic and evolutionary models, *Geology*, *27*, 499–502, doi:10.1130/0091-7613(1999)027<0499:DMYOGP>2.3.CO;2.

Werner, R., K. Hoernle, U. Barckhausen, and F. Hauff (2003), Geodynamic evolution of the Galápagos hot spot system (Central East Pacific) over the past 20 m.y.: Constraints from morphology, geochemistry, and magnetic anomalies, *Geochem. Geophys. Geosyst.*, *4*(12), 1108, doi:10.1029/2003GC000576.

White, R. S., D. McKenzie, and R. K. O'Nions (1992), Oceanic crustal thickness from seismic measurements and rare earth element inversions, *J. Geophys. Res.*, *97*, 19,683–19,715.

Wilkens, R. H., G. J. Fryer, and J. Karsten (1991), Evolution of porosity and seismic structure of upper oceanic crust: Importance of aspect ratios, *J. Geophys. Res.*, *96*, 17,981–17,995, doi:10.1029/91JB01454.

Ye, S., J. Bialas, E. R. Flueh, A. Stavenhagen, and R. von Huene (1996), Crustal structure of the Middle American Trench off Costa Rica from wide-angle seismic data, *Tectonics*, *15*, 1006–1021, doi:10.1029/96TC00827.

You, C. F., P. R. Castillo, J. M. Gieskes, L. H. Chan, and A. J. Spivack (1996), Trace element behavior in hydrothermal experiments: Implications for fluid processes at shallow depths in subduction zones, *Earth Planet. Sci. Lett.*, *140*, 41–52, doi:10.1016/0012-821X(96)00049-0.

Zelt, C. A., K. Sain, J. V. Naumenko, and D. S. Sawyer (2003), Assessment of crustal velocity models using seismic refraction and reflection tomography, *Geophys. J. Int.*, *153*, 609–626, doi:10.1046/j.1365-246X.2003.01919.x.